Earth Syst. Sci. Data, 17, 6025–6048, 2025
https://doi.org/10.5194/essd-17-6025-2025

Open Access Earth System Science Data

A dataset for multidisciplinary applications: thirteen years of ocean observations in Sermilik Fjord, Southeast Greenland

Aurora Roth[1], Fiamma Straneo[2,1], James Holte[2,1], Margaret Lindeman[2], and Matthew Mazloff[1]

[1]Scripps Institution of Oceanography, University of California at San Diego, La Jolla, CA, USA
[2]Harvard University, Cambridge, MA, USA

Correspondence: Aurora Roth (a1roth@ucsd.edu) and Fiamma Straneo (fstraneo@seas.harvard.edu)

Received: 12 June 2025 – Discussion started: 25 July 2025
Revised: 6 October 2025 – Accepted: 15 October 2025 – Published: 11 November 2025

Abstract. As global atmosphere and ocean temperatures rise and the Greenland Ice Sheet loses mass, the glacial fjords of Kalaallit Nunaat/Greenland play an increasingly critical role in our climate system. Fjords are pathways for freshwater from ice melt to reach the ocean and for deep, warm, nutrient-rich ocean waters to reach marine–terminating glaciers, supporting abundant local ecosystems that Greenlanders rely upon. Research in Greenland fjords has become more interdisciplinary and more observations are being collected in fjords than in previous decades. However, there are few long-term (> 10 years) datasets available for single fjords. Additionally, observations in fjords are often spatially and temporally disjointed, utilize multiple observing tools, and datasets are rarely provided in formats that are easily used across disciplines or audiences. We address this issue by providing standardized, gridded summer season hydrographic sections for Sermilik Fjord in Southeast Greenland, from 2009–2023. Gridded data facilitate the analysis of coherent spatial patterns across the fjord domain, and are a more accessible and intuitive data product compared to discrete profiles. We combined ship-based conductivity, temperature, and depth (CTD) profiles with helicopter-deployed eXpendable CTD (XCTD) profiles from the ice mélange region to create objectively mapped (or optimally interpolated) along-fjord sections of conservative temperature and absolute salinity. From the gridded data, we derived a summer season climatological mean and root mean square deviation, summarizing typical fjord conditions and highlighting regions of variability. This information can be used by model and laboratory studies, biological and ecosystem studies in the fjord, and provides context for interpreting previous work. Additionally, this method can be applied to datasets from other fjords helping to facilitate fjord intercomparison studies. The gridded data and climatological products are available in netCDF format at https://doi.org/10.18739/A28G8FK6D (Roth et al., 2025a). All original profile observations, with unique DOIs for each field campaign, are available through the Sermilik Fjord Hydrography Data Portal (https://arcticdata.io/catalog/portals/sermilik, last access: 7 November 2025) hosted by the Arctic Data Center (Straneo et al., 2025). The code used has also been made available to facilitate continued updates to the Sermilik Fjord gridded section dataset and applications to other fjord systems.

Published by Copernicus Publications.

1 Introduction

The glacial fjords of Kalaallit Nunaat/Greenland are key climate connectors – delivering freshwater (in liquid and solid form) to the ocean and warm ocean waters to the ice sheet. As global air and ocean temperatures rise and the Greenland Ice Sheet (GrIS) melts at an accelerating rate, understanding fjord variability is critical to addressing large-scale questions of GrIS mass loss, freshening of the North Atlantic, and potential global ocean circulation changes (Straneo and Cenedese, 2015). Locally, fjords are home to Greenlanders and their livelihoods are dependent on the future of fjords in our rapidly changing climate (Holm, 2010; Nuttall, 2020; Schiøtt et al., 2022). While abundant fjord ecosystems have been observed and utilized by Greenlandic peoples for thousands of years, there is increasing scientific interest for how physical fjord processes impact local ecosystems and biodiversity around Greenland and how these may evolve in a changing climate (Meire et al., 2017; Hopwood et al., 2020; Straneo et al., 2022).

Long-term and concurrent observations of atmosphere, glacier, ocean, and ecosystem variables at Greenland's coastal margins are essential for improving our understanding of glacial fjord systems. Motivated by science needs, the last decade has seen a significant increase in observations of all kinds collected in and near Greenland fjords. Notably, long-term (> 10 years) repeat oceanographic surveys have been carried out in Nuup Kangerlua (Godthåbsfjord) near Nuuk and in Young Sound in Northeast Greenland as part of the Greenland Ecosystem Monitoring MarineBasis Program (https://g-e-m.dk/gem-science-programme/marinebasis-programme, last access: 12 June 2025) and Greenland Institute of Natural Resources research campaigns (Juul-Pedersen et al., 2009; Mortensen et al., 2018). In Northwest Greenland, long-term oceanographic observations have been conducted in Kangerlussuaq (Inglefield Bredning) region near Qaanaaq (Sugiyama et al., 2020, 2025). Sermilik Fjord in Southeast Greenland, the focus of this study, has had nearly annual summer season oceanographic observations since 2008.

While many of the ice or atmospheric data at the margin of GrIS are available through remote sensing, reanalysis, or regional climate model products (e.g. Greenland Ice Sheet Mapping Project, ERA, RACMO), oceanographic data in fjords have been mostly collected by small research teams in isolated projects creating disparate datasets with widely varying characteristics distributed over many fjords (Schlegel and Gattuso, 2023). This makes it challenging to assemble these data in standard formats, typical of the large-scale oceanographic monitoring programs (e.g. ARGO, GO-SHIP), limiting their availability and usability.

Secondly, the environmental conditions and logistical constraints of working in fjords result in data being spatially and temporally disjointed. For example, repeat measurements at exact locations may be difficult to perform because of variable iceberg and sea ice presence and weather conditions. This makes it challenging to quantitatively compare different years or to provide modeling groups with mean properties instead of those based on a single survey. Even where repeat surveys exist, they may have been carried out using different instrumentation, sometimes within the same survey and/or by different groups over the years. Given the growing interest in understanding Greenland's fjords, it is important to develop data protocols and repositories that standardize fjord data from multiple surveys of a single fjord, facilitate comparisons between data collected in different fjords, and provide boundary conditions, forcings, and comparisons for ocean and ice sheet models (Juul-Pedersen et al., 2009; Straneo et al., 2019; Schlegel and Gattuso, 2023).

Finally, as Greenland fjord research becomes increasingly interdisciplinary and collaborations with local Greenlandic communities and government are being further strengthened, it is necessary that data be provided in formats that are accessible and usable by a wide range of users, including scientists from other disciplines (glaciologists, marine ecologists, social scientists), policy makers, educators, and local tourism operators.

Here, we present (1) a quality controlled hydrographic dataset from Sermilik Fjord in Southeast Greenland for 13 summer field campaigns occurring from 2009–2023, consisting of ship-based Conductivity, Temperature, and Depth (CTD) profiles and eXpendable Conductivity Temperature Depth (XCTD) profiles deployed from helicopters, (2) a standardized, gridded along-fjord section dataset (Roth et al., 2025a) combing both types of observations to increase usability by a diverse set of users, and (3) a summer climatological mean and root mean square deviation (RMSD), calculated from the gridded section dataset, summarizing the mean summertime fjord water properties and identifying regions with the greatest variability.

Data presented here include CTD profiles from ships and XCTD measurements typically deployed by helicopters in regions not accessible by ship. Some of these data have been described in previous studies (with data made available through data repositories) but the collective dataset and, importantly, the standardized gridded sections, which allow for survey–to–survey intercomparison and for the derivation of a robust summer season climatological mean, are new. Equally important, this study provides a procedure for the standardized gridding of the data, including an error estimate, where other observed variables in Sermilik Fjord (e.g. dissolved oxygen, nutrients) can easily be gridded and incorporated into the database by multiple users. The method can also be easily adapted and used to build gridded section datasets from profile observations in other fjord systems.

The gridded sections, created using an objective mapping method, facilitate the comparison of coherent spatial patterns between surveys, comparison to model output, comparison with other scattered observational variables, and can be used for calculating fjord transport quantities. They also address

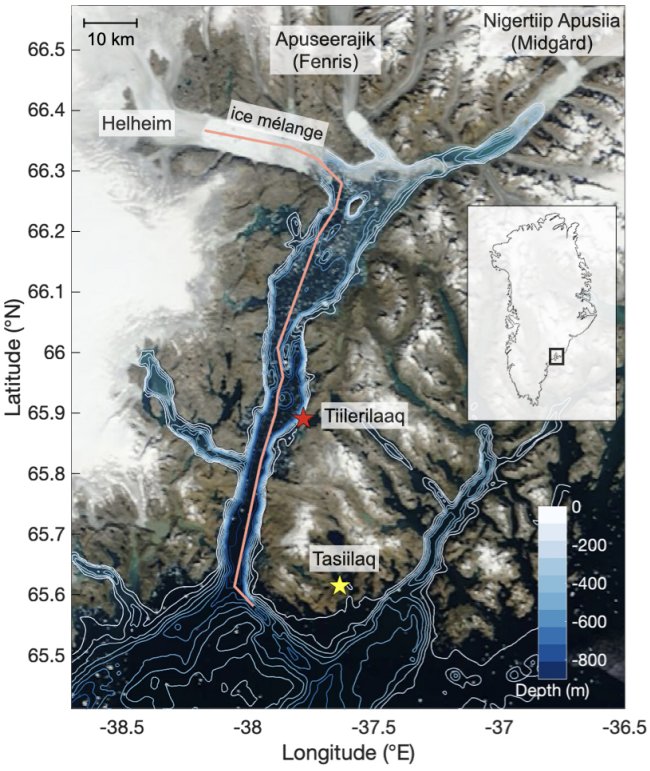

Figure 1. Map of Sermilik Fjord region in Southeast Greenland with major fjord branches and regions labeled. Bathymetry is shown as colored contours with 100 m increments and is derived from BedMachine Greenland v4 (Morlighem et al., 2017). The pink line represents the thalweg section of the fjord, used in plotting the bathymetry for the along-fjord sections (see text). The thalweg section end point is the Helheim Glacier terminus position in 2019. Background image is Terra MODIS corrected reflectance (true color) satellite image on 12 August 2023. This image was obtained from NASA Worldview Snapshot application (https://worldview.earthdata.nasa.gov, last access: 12 December 2024), part of Earth Science Data Information System (ESDIS).

the needs of interdisciplinary researchers not familiar with CTD and XCTD data processing or treatment of observations from discrete profiles, but who are interested in the mean and variable properties of the fjord for studies related, for example, to glaciers and ecosystems.

While more coordination and work is still needed within the science community, the approach shared here is a significant step toward creating a living data repository that standardizes long-term fjord observational records into a FAIR (Findable, Accessible, Interoperable, Reusable) data format to facilitate interdisciplinary research. The proposed framework for a larger, collaborative Greenland Ice Sheet-Ocean Observing System (GrIOOS) explicitly called for a repository such as this to facilitate the use of observations of Greenland's changing environment to address socially relevant questions at local to global scales (Straneo et al., 2019).

2 Sermilik Fjord setting

2.1 Glaciological context

Sermilik Fjord, located in southeast Greenland (Fig. 1), is long (∼ 90 km), narrow (5–10 km), and deep (550–900 m). The northern end of the fjord splits into three branching fjords with respective tidewater glaciers at the head of each branch – Helheim Glacier, Apuseerajik (Fenris Glacier), and Nigertiip Apusiia (Midgård, Midgaard, or Midgard Glacier) (Bjørk et al., 2015). Helheim, the largest of the three, is one of the largest and fastest flowing outlet glaciers of the GrIS. Due to Helheim's large volume of solid ice discharge, (∼ 30–38 Gt yr^{-1} since 2000 from Mankoff et al., 2020), freshwater input (∼ 500–650 m^3 s^{-1} peak freshwater discharge in July from Mankoff et al., 2020), and deep grounding depth (∼ 600 m) relative to the other glaciers, the physical dynamics of Sermilik Fjord are often studied by only considering the Helheim-Sermilik system. Since 2000, the terminus of Helheim has retreated ∼ 6 km and the glacier has lost an estimated 5–13 Gt yr^{-1} of ice (Williams et al., 2021). Similarly, Apuseerajik (Fenris) and Nigertiip Apusiia (Midgård) have had consistently negative annual mass balance and terminus retreats (∼ 4 and ∼ 11 km respectively) since 2000 (Williams et al., 2021; Huiban et al., 2024).

2.2 Regional ocean context

The properties and circulation of the Sermilik Fjord region have been described in a number of earlier studies, and are briefly summarized below to provide context for this dataset.

The mouth of Sermilik Fjord opens onto the continental shelf where the East Greenland Coastal Current (EGCC) flows south carrying cold Polar Water (PW) (Conservative Temperature (Θ) < 0 °C; Absolute Salinity (S_A) < 33.3 g kg^{-1}) of Arctic origin in the upper 200 m of the water column. Warmer, saltier Atlantic Water (AW) (Θ > 3 °C; S_A > 34.7 g kg^{-1}) from the Irminger Sea underlies the PW on the continental shelf (Harden et al., 2014). A trough (400–900 m deep) extending from the fjord mouth across the continental shelf allows for the warm AW to be funneled from the shelf into the fjord (Straneo et al., 2010, 2011; Sutherland et al., 2014b; Snow et al., 2023). Shelf waters transported by the EGCC are known to enter Sermilik Fjord following the trough on the East side of the mouth, while there is strong preferential out fjord flow on the western side (Sutherland et al., 2014a).

2.3 Sermilik Fjord water masses

The deep bathymetry of Sermilik Fjord with no shallow sills allows for direct exchange of PW and AW shelf waters (Fig. 1). As a result, the same two-layer structure can exist in the fjord with a pycnocline at 150–200 m depth. AW fills the deep regions along the entire length of Sermilik Fjord and is

present at the terminus of Helheim Glacier leading to submarine melting (Straneo et al., 2011). Regional wind dynamics on the shelf, primarily in the winter months during storms, result in oscillatory changes to the depth of the shelf pycnocline relative to the fjord, resulting in intermediary flow and fjord–shelf exchange (Jackson et al., 2014, 2018).

In the summer months, the addition of subglacial discharge, submarine meltwater, and surface runoff creates more complex fjord circulation, hydrography and ice–ocean dynamics. At glacier termini, buoyant subglacial discharge plumes entrain and upwell the deep, warm AW leading to enhanced submarine melting at the terminus and creating a water mass referred to as Glacially Modified Water (GMW). In Sermilik Fjord, GMW appears as a relatively warm and salty intrusion in the upper 50–250 m of the water column (Straneo et al., 2011; Beaird et al., 2018; Lindeman et al., 2024). At the surface (< 50 m), the submarine meltwater of icebergs and the addition of surface runoff creates a fresh anomaly, referred to as surface GMW (sGMW) (Straneo et al., 2011; Lindeman et al., 2024).

2.4 Helheim Glacier ice mélange

Helheim Glacier has a perennial ice mélange consisting of icebergs and sea ice (Fig. 1). The ice mélange region regularly extends up to 30 km from the Helheim terminus, however the total extent and area varies seasonally and interannually with changing glacier and calving dynamics (Foga, 2016; Harcourt et al., 2025; Meng et al., 2025). The submarine meltwater of icebergs in the mélange contributes to GMW and creates a cold temperature anomaly in the upper 100 m of the water column in the upper fjord area (Straneo et al., 2011; Enderlyn et al., 2016; Moon et al., 2018; Davison et al., 2022). Many questions remain about glacier–mélange–ocean feedbacks, in addition to questions about the role of subglacial discharge plumes in glacier–ocean dynamics at the terminus. Direct observations of these two fjord regions, ice mélange and subglacial discharge plume, are difficult and costly to obtain due to challenging ice conditions. The data presented here include observations from both regions for multiple summer seasons in Sermilik Fjord.

2.4.1 Sermilik Fjord Western science context

Sermilik Fjord became a site of intensive coordinated glaciological, atmospheric, and oceanic measurements starting in the late 2000s. Scientists aimed to understand the extent to which the ocean was playing a role in the retreat of Greenland's tidewater glaciers. At the time, there was little data from Greenland fjords and even high-resolution ocean models did not resolve fjord processes. Sermilik Fjord was chosen as a representative system of southeast Greenland glacial fjords because of the importance of Helheim Glacier to the dynamics of the GrIS as a whole (Straneo et al., 2016). More recently, Sermilik Fjord has been identified as a site for a Greenland Ice Sheet–Ocean Observing System (GrIOOS) due to the availability of interdisciplinary measurements previously collected there (Straneo et al., 2019).

Studies in Sermilik Fjord have greatly advanced our understanding of fjord systems and the role of fjord dynamics in connecting GrIS and the ocean. Important findings that have previously utilized portions of the CTD and XCTD hydrographic dataset presented here include (1) showing unequivocally that warm AW contacts glacier termini and drives submarine melting (Straneo et al., 2010, 2011, 2012), (2) demonstrating that glacial melt water entrains ambient fjord water and is exported out of fjords as GMW at depth (Straneo et al., 2011; Beaird et al., 2018), (3) teasing apart drivers of complex fjord circulation beyond traditional estuarine two layer circulation (Sciascia et al., 2013; Sutherland et al., 2014b; Jackson et al., 2014), (4) the importance of shelf processes for ice–ocean interactions in fjords (Jackson and Straneo, 2016; Spall et al., 2017; Sanchez et al., 2024; Snow et al., 2023), and (5) the role of icebergs and the ice mélange in freshwater export and fjord properties (Enderlyn et al., 2016; Moon et al., 2018; Davison et al., 2022; Hughes, 2022). The works listed have included analyses of these hydrographic data with other observational platforms in Sermilik Fjord (e.g. moorings) or are modeling studies using these hydrographic data for validation and/or forcing. Additionally, many advancements in our understanding of ice–ocean–climate processes as a whole have been made utilizing a wide range of datasets from the Helheim–Sermilik Fjord system from many different research groups.

More recently, the Sermilik Fjord region has been the site of studies addressing the relationships between physical ice and climate processes, fjord biogeochemistry, ecosystems, and local communities (Cape et al., 2019; Laidre et al., 2022; Straneo et al., 2022; Lindeman et al., 2024; Rathcke et al., 2025). Though specific project goals have varied over the years, CTD and XCTD surveys have been reliably conducted almost every summer since 2009, excluding 2014 and 2020 (Fig. 2; Tables 1 and 2). This dataset is one of the longest oceanographic records of summer season water properties inside a southeast Greenland glacial fjord.

3 Data

3.1 CTD data

We present data from summer surveys conducted from 2009 to 2023, except for 2014 and 2020 (Fig. 2; Tables 1 and 2). 364 shipboard CTD profiles and 71 XCTD profiles are included in this dataset. A variety of vessels and instrumentation have been used as methods, logistics, and instrument technology were improved and refined (Table 1). From 2009–2013, conductivity, temperature, and pressure observations were collected with RBR XR–620 Titanium CTDs sampling at 6 Hz. Instrument accuracy is reported by the manufacturer as $\pm 0.003\,\mathrm{mS\,cm^{-1}}$, $\pm 0.002\,^{\circ}\mathrm{C}$, and $\pm 0.05\,\%$ of

full depth scale for conductivity, temperature, and pressure sensors, respectively. Data from these CTDs required post–processing to correct unique pressure and conductivity offsets (Straneo et al., 2010). Conductivity, temperature, and pressure were aligned prior to calculating salinity to account for the fact that the sensors are not physically co–located on the logger. Data were manually examined to address any salinity spikes or anomalous points.

Starting in 2015, a Sea-Bird SBE19plus CTD was used as the primary instrument, sampling at 16 Hz. Instrument accuracy is similar to the RBR XR-620 CTD and reported to be $\pm 0.003\,\mathrm{mS\,cm^{-1}}$, $\pm 0.002\,^{\circ}\mathrm{C}$, and $\pm 0.1\,\%$ of full depth scale for conductivity, temperature, and pressure sensors, respectively. A RBR Concerto CTD was also mounted on the rosette and used for redundancy, with the same instrument accuracy as the RBR XR-620 and sampling at 16 Hz. SBE19plus CTD data were processed using Sea-Bird SBE data processing scripts to correct for lags between sensors, despike data, remove loops, and smooth data. Data were manually examined and any remaining anomalous points were removed.

All CTD profile data were vertically averaged to 1 m depth bins. We used the TEOS-10 Oceanographic Toolbox (McDougall and Barker, 2011) to convert in situ temperature to Conservative Temperature (Θ), conductivity to Absolute Salinity (S_A), and pressure to depth. All profiles were smoothed with a low-pass boxcar filter. The complete dataset of processed CTD profiles, grouped by cruise, are available with all metadata at the Arctic Data Center (https://arcticdata.io/catalog/portals/sermilik/Data, last access: 14 October 2025).

3.2 XCTD data

Starting in 2010, eXpendable Conductivity Temperature Depth (XCTD) probes were used in addition to shipboard CTDs (Straneo et al., 2011). The probes were deployed using helicopters to collect observations in the ice mélange and plume polynya regions where vessels cannot operate. Generally, the XCTD profiles are located in the near–terminus region of Helheim Fjord, but additional XCTD profiles have been collected in Midgård Fjord and the main branch of Sermilik Fjord in more recent years (Table 2).

XCTD instrument accuracy is reported as $\pm 0.03\,\mathrm{mS\,cm^{-1}}$, $\pm 0.02\,^{\circ}\mathrm{C}$, and $\pm 2.0\,\%$ of full depth scale for conductivity, temperature, and depth respectively. The depth measurements are based on a constant fall speed and are thus less accurate than shipboard CTDs measuring pressure directly. All XCTD profiles were manually inspected and anomalous data points were removed. We removed the top 4 m of each profile because it takes several seconds for the probe to equilibrate to the ocean temperature once it enters the water and begins recording. The bottom of each profile was manually identified by spikes in the conductivity measurements and cross-checked with expected bottom depth. The profiles were vertically averaged to 2 m depth bins to reduce noise. In situ temperature and conductivity were converted to Θ and S_A, respectively, using TEOS-10 Gibbs-SeaWater Oceanographic Toolbox (McDougall and Barker, 2011), and a low-pass boxcar filter was applied to each profile. These processed XCTD profiles are available for use and released with the same data and metadata format as the CTD profiles at the Arctic Data Center (https://arcticdata.io/catalog/portals/sermilik/Data, last access: 14 October 2025).

3.3 Combining CTD and XCTD data

XCTD measurements are less accurate compared to shipboard CTD measurements, and each XCTD profile uses a unique probe. Therefore we must consider whether any differences in measured water properties from each instrument type are due to biases in individual XCTD probes rather than real property variability. Because AW properties below 400 m have the smallest spatial and temporal variability throughout the fjord, we verified that the XCTD and CTD measurements for each year show matching AW properties within instrument error and known spatial variability, determined from the shipboard CTD measurements. No bias corrections were required for the XCTD data presented here, however, this is not always the case and this verification step is critical when working with combined XCTD and CTD data.

3.4 Profile locations and timing

There is a wide variety of profile locations and timing of the surveys during the summer season (Tables 1 and 2; Figs. 2 and 3). This is influenced by different logistical constraints and priorities of each field campaign and the fjord conditions at the time. The fjord has a high concentration of icebergs making exact repetition of profiling locations difficult. In general, an attempt is made each year to sample along the centerline of the fjord following the deepest bathymetric path (thalweg section) over a continuous time period (Fig. 1). Note that in 2009 and 2011 across-fjord sections were performed. From this data, it was determined that across-fjord variability is less significant compared to along-fjord variability, therefore surveys in the following years did not prioritize across-fjord sections (Straneo et al., 2011). Profiling locations are also influenced by recovering and deploying moorings, some of which are nearer to the coast than the fjord centerline. In 2018, the fjord survey was conducted in conjunction with specific iceberg surveys leading to many more profiles collected in the fjord that year. Other research priorities (e.g. biogeochemical sampling) for a given year have influenced the final pattern of profile locations within the fjord.

XCTD profile locations in the ice mélange are limited to where gaps exist between icebergs and sea ice to deploy the probe. Notably, in 2016 and 2019, the Helheim subglacial

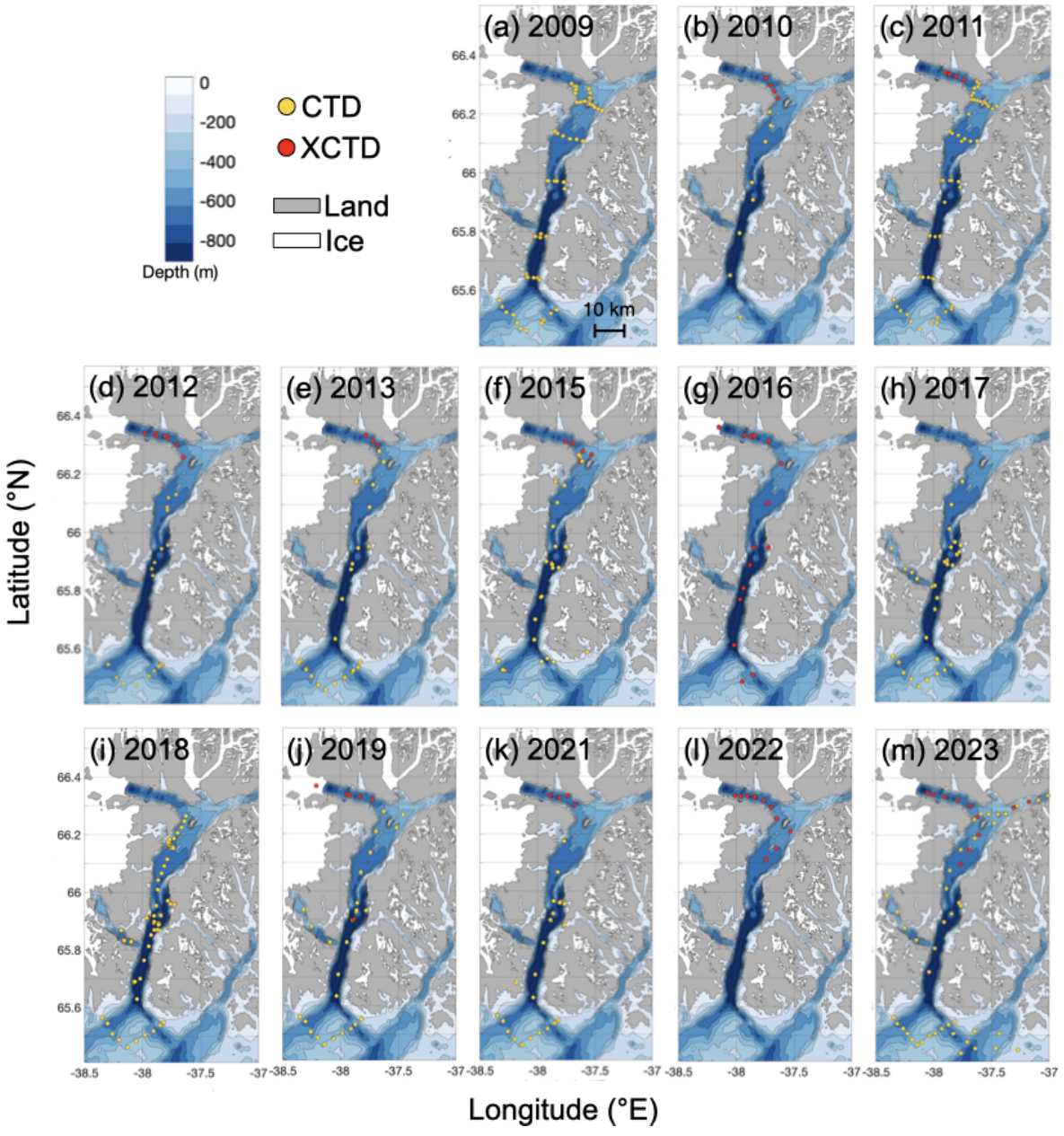

Figure 2. Locations of CTD (yellow dots) and XCTD (red dots) profiles for every summer survey in Sermilik Fjord included in this dataset. Bathymetry is shown as colored filled contours with 100 m increments. The bathymetry, land region, and ice regions are from BedMachine Greenland v4 (Morlighem et al., 2017). The land and ice regions correspond to outlines as they appear in the Greenland Ice Mapping Project (Howat et al., 2014) from the time periods 1999–2002 and 2013–2015. They are a static background for each year and do not represent specific ice extent and glacier terminus positions for a given year.

discharge plume was visible at the ocean surface (known as a plume polynya) and created ice-free openings (Melton et al., 2022). This allowed for the rare opportunity to deploy XCTD probes directly into the subglacial discharge plume waters at the glacier terminus, collecting observations of this undersampled and critical region. In 2016 and 2022, only helicopter-based XCTDs were used for the complete fjord survey due logistical constraints.

In contrast, the sampling locations on the shelf are repeated at nearly the same locations each year because icebergs are less present on the shelf. The V-shape configuration is designed to cross the trough twice, observing shelf waters flowing into the fjord using the East section and fjord waters flowing out of the fjord and onto the shelf using the West section. All shelf profiles have been processed as described

Table 1. Information about each shipboard CTD summer survey in Sermilik Fjord.

Year	Survey dates	Vessel	CTD instruments used	Number of fjord CTD profiles	Number of shelf CTD profiles
2009	19–25 August	MY *Arctic Sunrise*	XR 620 Titanium RBR (s/n 18559)	41	11
2010	22–27 August	*Pytur*	XR 620 Titanium RBR (s/n 18559)	7	1
2011	15–26 August	*Viking Mads Alex*	XR 620 Titanium RBR (s/n 18559)	39	12
2012	14–20 September	MV *Fox*	2 x XR 620 Titanium RBR (s/n 17413, 18559)	9	9
2013	18–28 August	*Viking Mads Alex*	2 x XR 620 Titanium RBR (s/n 17413, 18559)	13	14
2015	2–11 August	*Adolf Jensen*	SBEPLUS25 (s/n 251108); RBR Concerto (s/n 65584)	22	8
2017	15–22 July	*Adolf Jensen*	SBEPLUS25 (s/n 251108); RBR Concerto (s/n 65584)	21	10
2018	3–14 August	*Adolf Jensen*	SBEPLUS25 (s/n 251108); RBR Concerto (s/n 65584, 66129); RBR XR Titanium (s/n 18608)	60	10
2019	27 July–1 August	*Adolf Jensen*	SBEPLUS25 (s/n 251108); RBR Concerto (s/n 66130)	16	10
2021	10–18 August	*Adolf Jensen*	SBEPLUS25 (s/n 251108); RBR Concerto (s/n 66130)	15	12
2023	5–19 August	RV *Tarajoq*	SBEPLUS25 (s/n 251108); RBR Concerto (s/n 66130)	16	12

Table 2. Information about each XCTD survey in Sermilik Fjord. * One winter survey was conducted on 15–16 March 2010 (Straneo et al., 2011). These profile data are available, but have not been gridded or included in the summer season climatology.

Year	Survey dates	Total number of XCTD profiles	Number of XCTD profiles in ice mélange
2010*	15–16 March	5	1
2010	26 August	4	4
2011	26 August	4	4
2012	14 September	7	7
2013	22 August	3	3
2015	27 July	5	5
2016	9–11 August	16	6
2019	31 July, 6 August	7	6
2021	11 August	4	4
2022	11 September	10	6
2023	12 July	12	5

in Sect. 3.1 and are available with their associated fjord profiles for each year.

The surveys have occurred at different time periods in the summer season (Fig. 3). The seasonal dynamics of the fjord evolve over time and summer conditions can vary widely. Subglacial discharge and surface runoff begin to enter the fjord in June after the onset of the surface melt season. Both forms of freshwater entering the fjord peak in volume flux in late July and are usually negligible by late October (Mankoff et al., 2020). Buoyancy-driven circulation takes some time to set up with the addition of subglacial discharge. The continued addition of subglacial discharge throughout the summer can change the overall fjord stratification, altering the neutral buoyancy depth of the subglacial discharge plume over a summer season (Sanchez et al., 2023). Each year the surveys are capturing different time periods in this overall seasonal evolution of the fjord. Additionally, wind events on the shelf can drive shorter timescale (days to weeks) intermediary circulation on top of the buoyancy-driven circulation (Jackson et al., 2014, 2018). These events can quickly change fjord water mass properties over the timescale of a single fjord survey. Understanding the field campaign timing relative to freshwater inputs, wind conditions, regional climate conditions, is critical context for interpreting the data presented here.

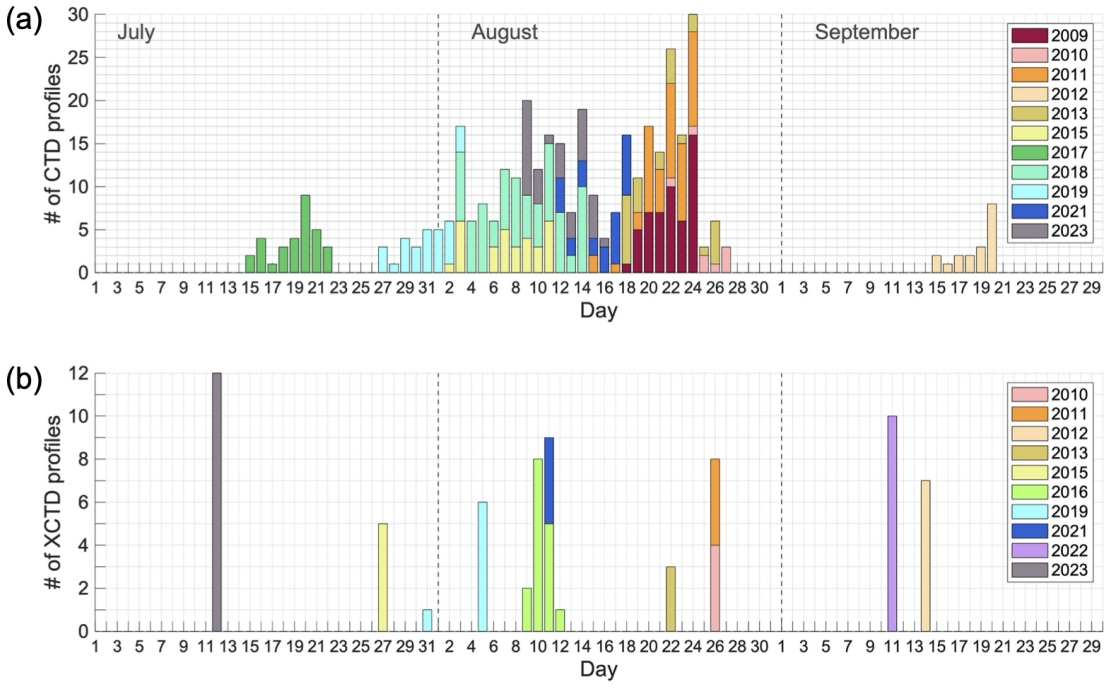

Figure 3. A visual representation of the survey dates and time periods in the summer season (July–September). Number of CTD (top) and XCTD (bottom) profiles collected on each day in the summer survey period across all years. Bar colors represent individual years. Dashed grey vertical lines denote the start/end of a month.

4 Methods

4.1 Profile selection for analysis

Prior to the gridding process, we constructed along-fjord sections for each survey following the thalweg transect line (Fig. 1). This required careful manual selection of profiles located nearest to the thalweg line and capturing similar fjord conditions within a certain time period. If profiles in similar locations existed, but were collected at different time periods during the survey (e.g. collected while sailing upfjord and then downfjord several days later), we only retained the profile that created the best continuous synoptic section. If multiple profiles were collected in the across-fjord direction at the same along-fjord distance then those across-fjord profiles were averaged and the mean profile was used in the along-fjord section. Profiles near the shallower (< 300 m) fjord sides were not included. The final selection of individual profiles and mean profiles (averaged in the across-fjord direction) making up the best synoptic along-fjord hydrographic section were then used as input data to create the gridded along-fjord dataset.

Data from inside the plume regions from years 2016 and 2019 are not included in the along-fjord sections. This is because the gradients of properties are at a finer scale in this dynamic region than we are accounting for in the objective mapping process. These plume data are discussed separately. Similarly, dynamics in the shelf region occur at different scales compared to the fjord and we do not use the shelf profiles for constructing the fjord sections.

Prior to objective mapping, we perform a "bottom fill" procedure for profiles extending beyond 550 m or deeper to enhance data density of the deep fjord regions for the objective mapping process. For all profile locations, properties below the sill depth of 550 m show little variability and are remarkably stable with respect to depth, but they do vary in the along-fjord distance. Without bottom filling of these profiles, the deepest profile informs the properties at that depth across the fjord when it is more likely that properties are similar to their nearest vertical neighbors. First, for all profiles extending 550 m or deeper, we calculated the average temperature and salinity value of the deepest 10 m of that profile. Then, we extrapolated these properties uniformly to the bottom. This extrapolation procedure was used for 128 profiles out of a total of 172 used in the along-fjord sections.

4.2 Creating gridded data using objective mapping

The challenge of creating gridded fields from scattered observations is well known in the earth sciences and there are many possible approaches. Objective mapping (also referred to as optimal or optimum interpolation) allows for the explicit use of input parameters and use of multiple spatial correlation scales to better represent physical processes. Objective mapping approaches are commonly applied to other hydrographic profile datasets including from the northern

Antarctic Peninsula (Dotto et al., 2021) and the Weddell Sea (Reeve et al., 2016), and of biogeochemical profiles in the Southern Ocean (Mazloff et al., 2023). These previous applications are concerned with larger ocean basin-scale observations, often involving thousands of profiles, and spanning decades. This is the first application of objective mapping for a Greenland fjord. Only recently have we been monitoring Sermilik Fjord long enough (> 10 summer seasons) and with dense enough observations to appropriately inform the parameters and assumptions of the interpolation method. The increased utility provided by a gridded section dataset became apparent as research about Greenland fjords is maturing and data volume is increasing. We note that our use of "gridded data" here refers to gridded hydrographic sections (or transect) using a 2D coordinate system consisting of an along-fjord horizontal direction and depth. This is in contrast to other forms of gridded data with a 3D coordinate system (e.g. outputs of regional ocean models using latitude, longitude, and depth levels) or a map view 2D coordinate system of latitude and longitude (e.g. satellite data).

The along-fjord sections constructed with the final selected discrete profiles for each year were mapped onto a 2 km (horizontal) × 5 m (vertical) grid with the objective mapping procedure. The horizontal along-fjord coordinate system is referenced using 0 km at the 2019 location of Helheim Glacier's terminus and follows the thalweg section line. Associated latitude and longitude coordinates of gridcells this transect are included in the data products. The gridding process was performed independently for temperature and salinity variables. While each section is ultimately mapped to the same grid cell locations, the data extent of each gridded section varies because they are bounded by the minimum and maximum along-fjord distance locations of the profiles in each survey. The deepest vertical extent of each gridded section is bounded by the maximum depth profile for each survey (Fig. 4).

4.2.1 Objective mapping algorithm

First, a background field across the full domain (also referred to as a "first guess") was created by considering all summer season profiles selected by the process described above. The resulting background field, $\boldsymbol{g}_\mathrm{b}$, represents the large-scale field which is well determined by the data and horizontal sampling locations.

For each year, the data anomaly $\boldsymbol{d}'$ was calculated as

$$\boldsymbol{d}' = \boldsymbol{d} - \mathbf{H}\boldsymbol{g}_\mathrm{b} \tag{1}$$

where $\boldsymbol{d}$ is a vector of the original profile data for one year with n number of total data points at unique locations (x_i, z_i). $\mathbf{H}$ is a matrix operator that linearly interpolates $\boldsymbol{g}_\mathrm{b}$ to the same spatial coordinates as the original data points of $\boldsymbol{d}$.

The data anomalies for each year, $\boldsymbol{d}'$, are then objectively mapped using the gain matrix, $\mathbf{K}$, to produce the final gridded field by adding the background field, $\boldsymbol{g}_\mathrm{b}$, back to produce the final gridded field, $\boldsymbol{g}_\mathrm{a}$ (Eq. 2). It is common practice to objectively map the anomaly field (Bretherton et al., 1976; Roemmich, 1983). Prior to being mapped using Eq. (2), the anomaly data, $\boldsymbol{d}'$, were normalized by the standard deviation and the mean was subtracted.

The gridded field for each year, $\boldsymbol{g}_\mathrm{a}$, is produced by

$$\boldsymbol{g}_\mathrm{a} = \mathbf{K}\boldsymbol{d}' - \boldsymbol{g}_\mathrm{b}. \tag{2}$$

The gain matrix, $\mathbf{K}$, objectively maps the data anomalies, $\boldsymbol{d}'$, and the background field is added back in. The core part of the objective mapping procedure is $\mathbf{K}$ (Ide et al., 1997). It's also referred to as the coefficient or weighting matrix (Wong et al., 2003; Reeve et al., 2016). $\mathbf{K}$ is constructed using the data-data spatial covariance matrix, $\mathbf{C}_\mathrm{dd}$, and the data-grid spatial covariance matrix, $\mathbf{C}_\mathrm{dg}$, where

$$\mathbf{K} = \mathbf{C}_\mathrm{dg} \cdot [\mathbf{C}_\mathrm{dd} + \mathbf{R}] - 1. \tag{3}$$

We assume the covariances are each a sum of a large-scale Gaussian and a small-scale Gaussian (Eqs. 4 and 5). The decay scales of each Gaussian are determined by four scale parameters: large- and small-scale horizontal correlation scales, L_{x_1} and L_{x_2}; and large- and small-scale vertical correlation scales, L_{z_1} and L_{z_2}. Each Gaussian has an amplitude parameter which determines the relative weighting of the large-scale (A_1) and small-scale (A_2) functions in the final map. The sum of A_1 and A_2 must be equal to 1 and must both be positive values. These six parameters were prescribed and determined by prior knowledge of scales of variability in the system, and tuned such that they yield a realistic field that best captures the conditions and dynamics of the fjord.

$$\begin{aligned}\mathbf{C}_{\mathrm{dd}_{ij}} = {} & A_1 \cdot \exp\left\{ -\left[\frac{\mathrm{dist}_{x_{ij}}^2}{L_{x1}} + \frac{\mathrm{dist}_{z_{ij}}^2}{L_{z1}} \right] \right\} \\ & + A_2 \cdot \exp\left\{ -\left[\frac{\mathrm{dist}_{x_{ij}}^2}{L_{x2}} + \frac{\mathrm{dist}_{z_{ij}}^2}{L_{z2}} \right] \right\}\end{aligned} \tag{4}$$

$$\begin{aligned}\mathbf{C}_{\mathrm{dg}_{ig}} = {} & A_1 \cdot \exp\left\{ -\left[\frac{\mathrm{dist}_{x_{ig}}^2}{L_{x1}} + \frac{\mathrm{dist}_{z_{ig}}^2}{L_{z1}} \right] \right\} \\ & + A_2 \cdot \exp\left\{ -\left[\frac{\mathrm{dist}_{x_{ig}}^2}{L_{x2}} + \frac{\mathrm{dist}_{z_{ig}}^2}{L_{z2}} \right] \right\}\end{aligned} \tag{5}$$

The data-data spatial covariance matrix, $\mathbf{C}_\mathrm{dd}$,is a function of the distances between every i data point location to every other j data point location in the horizontal ($\mathrm{dist}_{x_{ij}}$) and depth ($\mathrm{dist}_{z_{ij}}$) directions. $\mathbf{C}_\mathrm{dd}$ is thus a $n \times n$ square matrix where n is the number of original data points. The diagonal values of this matrix are 1 as this represents the distance of each profile data point to itself. The data-grid spatial covariance matrix, $\mathbf{C}_\mathrm{dg}$, is a function of the distances between every i data point location to every g grid point location in the final gridded domain. $\mathbf{C}_\mathrm{dg}$ is an $m \times n$ matrix where m is the total number of grid point locations.

To represent noise in the system, we define the noise matrix, $\mathbf{R}$, as

$$\mathbf{R} = \epsilon^2 \cdot \mathbf{I}. \quad (6)$$

The value of ϵ^2 is a prescribed noise-to-signal parameter of the data anomalies. A larger value of ϵ means that the map is less able to represent the data anomalies and the final map is less influenced by those data values because more "noise" is assumed to exist in the system. The choice of ϵ strongly impacts the final map (Mazloff et al., 2023). Our choice here is $\epsilon = 0.5$ times the standard deviation of the data anomalies, $\boldsymbol{d}'$, and this is a parameter that can be adjusted depending on application or the question of interest. $\epsilon = 0$ would represent that the values of the final map at the data locations must be equal to the original data values. However, it is not possible to use $\epsilon = 0$ because the sum of $\mathbf{C}_{\mathrm{dd}} + \mathbf{R}$ in Eq. (3) produces a non-zero diagonal for the matrix inversion, which is mathematically necessary for this objective mapping procedure. A non-zero value for ϵ acknowledges that we are modeling the system with smoothness at the lengthscales specified in Eqs. (4) and (5) and signals at smaller scales than these are considered "noise" not represented by the chosen lengthscale parameters.

Objective mapping allows for the calculation of the error variance of the gridded field as

$$\boldsymbol{\sigma}_g^2 = \mathrm{diag}(\mathbf{I} - \mathbf{C}_{\mathrm{dg}} \cdot [\mathbf{C}_{\mathrm{dd}} + \mathbf{R}]^{-1} \cdot \mathbf{C}_{\mathrm{dg}}^T) \cdot \boldsymbol{\sigma}_d^2. \quad (7)$$

$\boldsymbol{\sigma}_d^2$ is the variance of the original data, $\boldsymbol{d}$. We report uncertainty in units of the observed data by taking the square root of Eq. (7). We share the gridded fields of the uncertainty (also referred to as mapping relative error) so that a user can gauge the amount of uncertainty in the map.

After deriving the gridded fields, we apply a correction to the temperature field. For the coldest temperatures at the freezing point of seawater with limited data points nearby, the objective mapping procedure interpolates the gridded temperature to be colder than the freezing point. We identify these values and correct them to be at the freezing point of seawater, calculated using the gridded salinity value of that gridded data point. This correction was applied to 27 out of 77 521 total gridded data points in all the final gridded temperature fields.

4.3 Choosing a background field

The background field, $\boldsymbol{g}_{\mathrm{b}}$, is an important parameter in the objective mapping method and can be constructed in a number of ways. The constant hydrographic features we aimed to capture in a background field were the two-layer temperature structure of the fjord (cold water on top of warmer water), colder surface waters in the ice mélange relative to the mouth, and a large salinity range with nearly fresh water at the surface and increased salinity with depth. For both temperature and salinity fields, we plotted all selected along-fjord profiles from every summer season in the fjord onto one along-fjord axis, linearly interpolated these profiles to the 2 km × 5 m standardized grid. We then heavily smoothed this grid in the vertical and horizontal using a boxcar filter to achieve the desired large-scale background field features. We explored alternative methods for choice of background field, including creating individual background fields for every year from linearly interpolating between spatial endmember profiles closest to the glacier and mouth. We determined that any reasonable method for creating a background field that results in a representation of the average large-scale hydrographic features described above leads to similar objective mapping performance.

Table 3. Description of assigned parameters in objective mapping method.

L_{x_1} (km)	L_{z_1} (m)	A_1	L_{x_2} (km)	L_{z_2} (m)	A_2	ϵ
50	100	0.6	15	10	0.4	0.5

4.4 Choosing appropriate parameters

In the objective mapping method used here, there are seven parameters chosen based on knowledge of the system and the observations (Table 3). The same parameters were used for every year and for both temperature and salinity fields. Other applications of objective mapping in fjords could use more or fewer Gaussian lengthscale functions with different values and relative weights in order to capture the dynamics of a specific system. Initial lengthscale values were tested based on visual inspection of the scattered data and an error value was chosen informed by previous objective mapping applications and known instrument error (Dotto et al., 2021; Mazloff et al., 2023). Following other studies, we performed a series of tests exploring the parameter space to choose a parameter combination that yielded minimized residual values and an appropriate representation of smoothed hydrographic features for the whole domain each summer. By making the code for this method available, we stress that others can adjust parameters to produce gridded fields that best match features of interest within Sermilik Fjord or best match features in other fjords with different spatial patterns.

4.5 Calculating a climatology

We calculated a climatology representing the average summer state properties of Sermilik Fjord from the summer along-fjord gridded sections. For both temperature and salinity, the mean and root mean square deviation (RMSD) at every grid cell was calculated. The 2009–2023 grids for each survey cover different fjord extents based on the locations of the original profiles for each year. As a result, each grid cell mean and RMSD was calculated from a different number of

years ranging from 1–14 (Fig. 4). The 2023 CTD and XCTD data are not combined and treated as two separate instances of a summer fjord state, yielding a maximum of 14 available grids to be used in calculating each grid cell mean. Grid cells between 40–50 km from the terminus use all 14 grids while grid cells 12 km from the terminus only have 3 grids to calculate the mean. This reflects the challenge of obtaining repeat observations in the ice mélange region. Grid cells with fewer than 3 years were not included in the final climatology.

5 Results

5.1 Objective mapping performance

We judged the parameter choice performance based on the root mean squared error (RMSE) values, the pattern of residuals across the domain, and the visual representation of hydrographic features in the final gridded fields. Residuals were calculated by subtracting the gridded value from the observed value, where the gridded data were linearly interpolated to match the exact along-fjord and depth coordinates of each observed data point. The gridded temperature fields at the profile locations, residuals at those locations, and the associated temperature relative mapping error for the years 2009 and 2019 are shown in Fig. 5a–f. We highlight these two years with differing hydrographic patterns and spacing between profile locations to demonstrate the objective mapping performance across a range of input profile data characteristics.

We evaluated the residuals and RMSE for each survey individually and across all surveys in bulk for both temperature and salinity fields. For the final parameter set presented here for all surveys, 88 % of temperature residuals are within a difference range of ± 0.1 °C and 67 % are within a difference range of ± 0.04 °C. 91 % of salinity residuals are within a difference range of $\pm 0.05\,\mathrm{g\,kg^{-1}}$ and 77 % are within a range of $\pm 0.02\,\mathrm{g\,kg^{-1}}$ (Fig. 6). The bulk RMSE is 0.09 °C and $0.08\,\mathrm{g\,kg^{-1}}$, for temperature and salinity respectively. The observed salinity profiles are more spatially smooth compared to the temperature profiles resulting in slightly smaller RMSE values.

The pattern of residuals across the domain is equally important to understand which hydrographic features are and are not represented well in the interpolation method. Sharp thermoclines within the upper 200 m at length scales smaller than the prescribed vertical smoothing ($L_{x_2} = 10$ m) result in the highest residual values in the domain. These are often present near the fjord mouth where interleaving of different water masses between the fjord and shelf is known to occur. High residuals also consistently occur in the ice mélange region at ~ 150 m depth where there is a sharp thermocline transition between cold ice mélange meltwater and warmer waters at depth.

We also provide the mapping relative errors in the same format as the temperature and salinity gridded sections. The user is able to choose a relative error value to work with, if needed. The mapping relative error magnitudes of all sections are acceptable for most use cases as shared here. Considering all sections, the range of error is 0.03 to 0.30 °C and 0.04 to $0.40\,\mathrm{g\,kg^{-1}}$ for the temperature and salinity grids respectively. As expected, the error increases as the distance between data points increases beyond the lengthscale parameters.

Finally, parameter choice was aided by visual inspection of the original profiles and gridded data for each year in Θ–S_A diagrams (Fig. 7). This was to ensure that the gridded sections did not introduce density classes beyond the range present in the observations. The final parameter set shows good agreement between the gridded data and observations in Θ–S_A space.

5.2 Climatology and spatial variability

The complete set of Θ and S_A along-fjord gridded sections are available to view in the Supplement (Figs. S1–S8). Combining the CTD and XCTD datasets extends the along-fjord spatial coverage for years where both types of profiles were collected concurrently. Despite differences in original profile locations and fjord coverage from year to year, the standardized gridded along-fjord sections allow us to calculate a summer state climatology and associated RMSD for the Helheim–Sermilik Fjord system (Fig. 8). This is one example of the increased utility of the gridded dataset compared to utilizing individual surveys or less explicit interpolation methods. The climatology product provides novel context for the yearly variability of summer season fjord water properties and improves the interpretation of previously published work from Sermilik Fjord.

Typical of Greenland glacial fjords, the climatology shows salinity is the dominant driver of stratification. The basic salinity structure is consistent throughout the fjord, with a maximum salinity of $34.95\,\mathrm{g\,kg^{-1}}$ below 400 m, gradually freshening toward $34.40\,\mathrm{g\,kg^{-1}}$ at 200 m depth (Fig. 8b). The halocline steepens in the upper 200 m, with the surface layer having the sharpest vertical salinity gradients over the entire along-fjord extent.

Below 400 m, temperature is also relatively uniform along the length of the fjord (Fig. 8a). The mean properties of this layer (3.81 ± 0.15 °C, $34.89 \pm 0.04\,\mathrm{g\,kg^{-1}}$, potential density anomaly $\sigma_0 > 27.5\,\mathrm{kg\,m^{-3}}$) are consistent with established characteristics of inflowing AW from the continental shelf (Straneo et al., 2011; Jackson and Straneo, 2016; Beaird et al., 2018; Lindeman et al., 2024).

Above 400 m, we see more spatial variability in temperature indicative of different water masses and ice–ocean processes. To identify characteristics of along-fjord variability above 400 m, we have separated the fjord into three regions based on the water mass properties and established process understanding. We proceed by first describing water properties at the mouth region where we expect the fjord to be

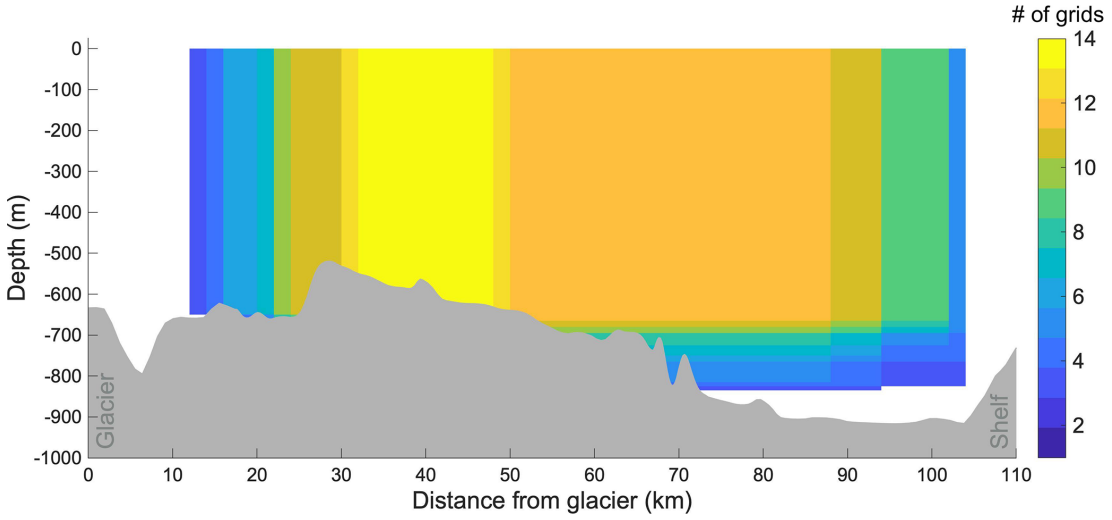

Figure 4. The number of grids representing each survey that have data in each grid cell in the along-fjord standardized grid domain. The number in each grid cell is used to calculate the property mean and RMSD. Grid cell size is 2 km (horizontal) by 5 m (vertical). Grid cells with only 1 or 2 surveys of coverage have been removed.

influenced by exchanges with the shelf. Second, we describe the near glacier region and address the glacial forcing on water properties, and finally we describe the mid-fjord region which shows gradients between the mouth and near glacier water properties.

5.2.1 Fjord mouth properties

At the fjord mouth (averaged over 94–104 km from the glacier), we see a mean temperature structure similar to the established, typical summer properties on the continental shelf nearby. A thermocline centered on the 27 kg m^{-3} isopycnal separates a subsurface temperature minimum from the underlying warm AW. The AW properties at the mouth vertically averaged between 400–700 m are 3.85 ± 0.13 °C and 34.88 ± 0.04 g kg^{-1}.

In the upper water column, there is a subsurface temperature minimum (50–100 m, $\sigma_0 = 26.5$ kg m^{-3}) below a near-surface warm layer. This subsurface temperature minimum is at a similar depth and density to the cold, unmodified PW layer typically observed on the shelf (Sutherland and Pickart, 2008). However, the fjord mouth subsurface temperature minimum is 1 °C warmer than the established properties of unmodified shelf PW (< 0 °C).

To better interpret the properties at the fjord mouth, we identified unmodified PW properties from shelf profiles included in this dataset. Shelf profiles were collected during each survey, but are not included in the creation of the gridded data for the fjord. We created a single representative shelf profile for each survey by taking the temperature minimum of each isopycnal band across all East section shelf profiles, which sample the inflowing shelf waters, for a given survey (Fig. 7). We then calculated a mean profile from all representative East section shelf profiles from each survey. The subsurface temperature minimum of the mean profile indicates the coldest unmodified PW present on the shelf, on average, across all surveys from 2009–2023 and is comparable to the fjord summer climatology properties (Fig. 9). The mean East shelf coldest PW properties are -1.22 ± 0.35 °C and 33.17 ± 0.25 g kg^{-1}, occurring at a mean depth of 77 m and ranging from 50–115 m depth. These properties agree with previous observations of unmodified PW on the shelf outside of Sermilik Fjord (Sutherland and Pickart, 2008; Harden et al., 2014). However, the properties we calculated here are representative of more surveys allowing for improved understanding of the stability and variability of PW properties, and their influence on fjord properties. From this brief analysis, we can conclude that, on average, the temperature minimum at the fjord mouth in the 50–100 m layer represents a mixture of PW and fjord-origin GMW that is nearly 1.5 °C warmer than unmodified shelf PW.

5.2.2 Near glacier properties

In the near glacier ice mélange region (horizontally averaged between 12–22 km from the glacier), the climatological mean AW properties vertically averaged between 400–700 m are 3.59 ± 0.17 °C and 34.84 ± 0.05 g kg^{-1}, within one standard deviation of the properties at the mouth.

Above the AW layer, the near glacier region has a positive temperature anomaly when compared to the mouth (between 75–300 m) and shelf (between 55–300 m), calculated by subtracting along isopycnals. The temperature anomaly and features of the near glacier profiles in Θ–S_A space (Fig. 9) are characteristic of GMW (Straneo et al., 2011; Muilwijk et al., 2022). Building on previous work, we can identify the fin-

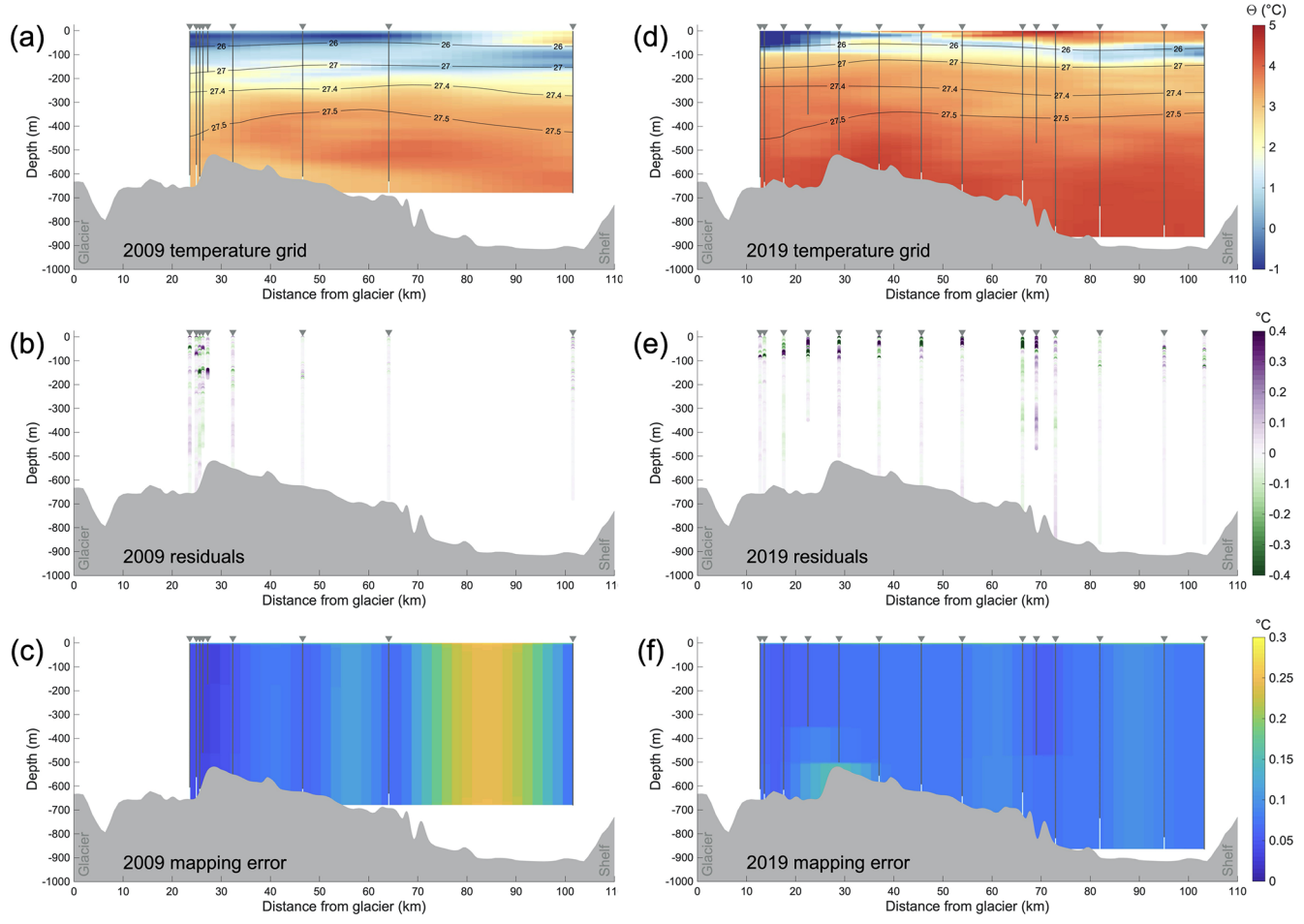

Figure 5. The conservative temperature objectively mapped gridded fields for 2009 **(a)** and 2019 **(d)** with potential density anomaly isopycnals (black contours). Original CTD and XCTD profile locations in the along-fjord direction are shown by triangle markers with vertical black lines representing the depth extent of each profile. White lines show where the bottom of a profile was filled in to facilitate greater data coverage for mapping. The 2009 **(b)** and 2019 **(e)** residual values are shown by filled dots at each original data point. The mapping relative error **(c, f)** is shown for each year. The bathymetry (grey area) is derived from a thalweg line (Fig. 1) of BedMachine Greenland v4 data (Morlighem et al., 2017). Distance 0 km is the location of the Helheim Gletsjer terminus in 2019.

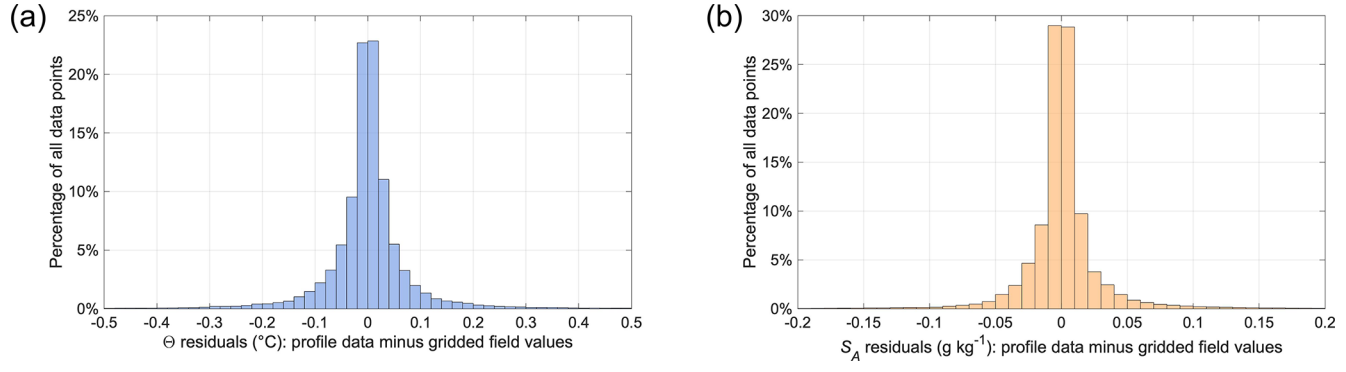

Figure 6. Histograms displaying the distribution of residual values between the gridded temperature **(a)** and salinity **(b)** fields and the profile observations considering all years in bulk. Bin size is 0.02 °C **(a)** and and 0.01 g kg^{-1} **(b)**.

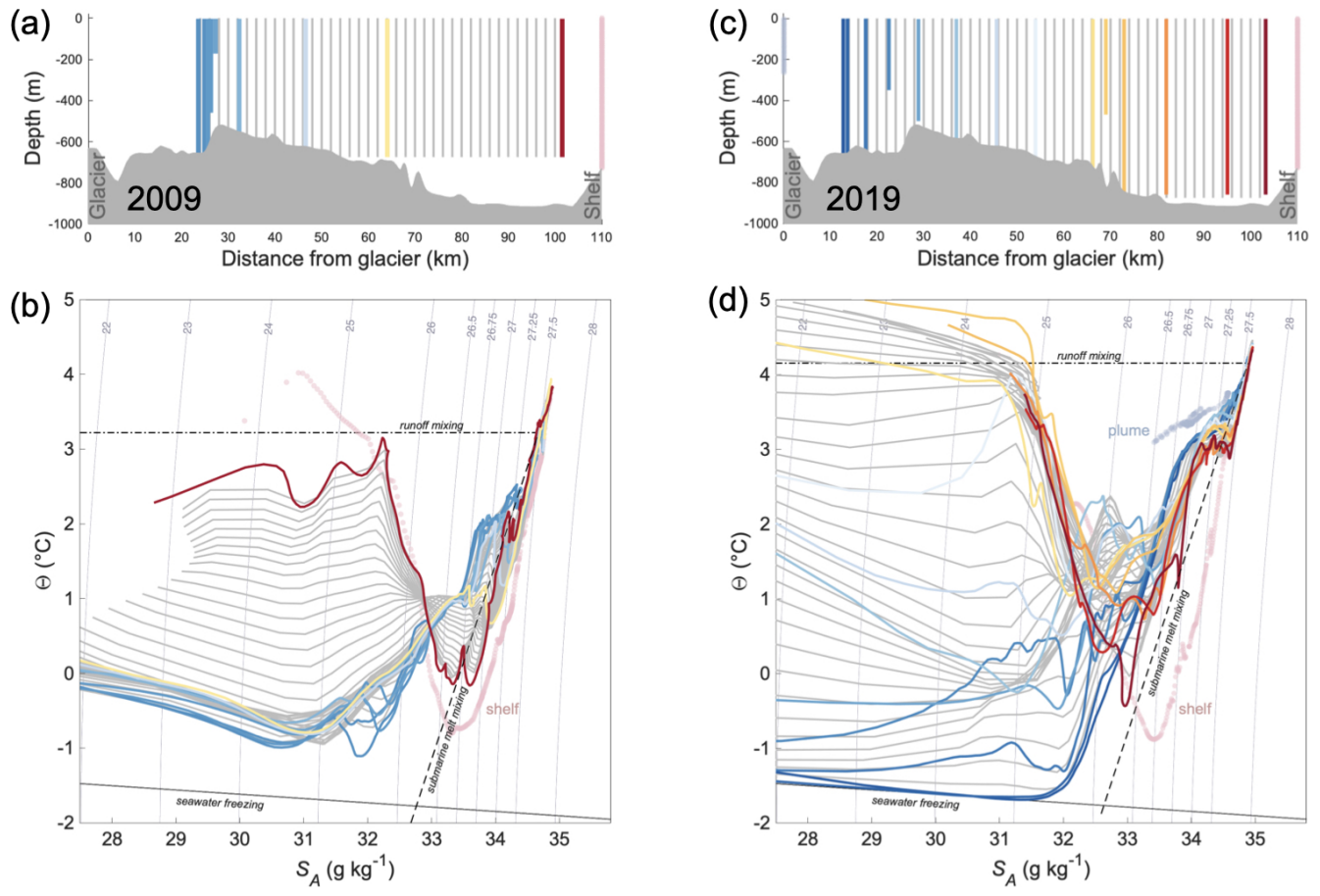

Figure 7. Comparisons of original profiles and gridded data for years 2009 **(a, b)** and 2019 **(c, d)** in Θ–S_A diagrams **(b, d)**. Panels **(a)** and **(c)** show the along-fjord location of the original profiles, colored by distance from the glacier, in comparison to location of the grid cells (grey lines). Θ–S_A diagrams **(b, d)** show original profiles, colored by distance from the glacier in panels **(a)** and **(c)**. Grey lines are the gridded data with every column in the grid plotted as an individual profile. Shelf profiles from both years are shown in light pink and two plume profiles from 2019 are shown in light blue. Mixing lines are plotted for submarine ice melt (dashed line) and melt runoff (dot-dash line) and the seawater freezing line is the black solid line. Grey contours are potential density anomaly isopycnals in kg m^{-3}.

gerprints of different freshwater sources and determine their relative importance for setting the GMW water properties throughout the fjord.

We use the mixing lines displayed on the Θ–S_A plot to differentiate between SGD, surface runoff, or SMW influence (Fig. 9). The runoff mixing line shown represents the expected water properties for the mixing of averaged unmodified AW at 550 m and SGD (with assumed properties of 0 °C and 0 g kg^{-1}). The SMW mixing line, or Gade line, represents the combined influence of latent heat uptake and mixing with meltwater (Gade, 1979). The two XCTD profiles collected directly in the plume at the glacier terminus from 2016 and 2019 strongly parallel the runoff mixing line slope. Between 165–300 m ($27.22\,\mathrm{kg\,m^{-3}} < \sigma_0 < 27.49\,\mathrm{kg\,m^{-3}}$), the slope of the near glacier profiles (20 km from the glacier terminus; dark blue profiles in Fig. 9) deviate in the composite direction of the runoff mixing line and submarine melt line. This is consistent with a mixture of plume waters and SMW from the ice mélange. The inflection of the slope at depths shallower than 165 m ($\sigma_0 < 27\,\mathrm{kg\,m^{-3}}$) suggests that this is the upper limit of SGD, which can be used as an estimate of the climatological average neutral buoyancy depth range of plume waters in this region of the fjord.

Between 50 and 165 m ($26.0\,\mathrm{kg\,m^{-3}} < \sigma_0 < 27.22\,\mathrm{kg\,m^{-3}}$), the slopes of the near glacier profiles directly parallel the submarine melt mixing line, indicating the addition of SMW from the ice mélange as a primary driver of water properties at these depths. Above 50 m, the Θ–S_A properties converge toward the local freezing temperature as the near surface waters are both cooled by SMW and freshened by surface runoff. The surface water properties nearest to the glacier (12 km) are the coldest in the entire domain, with a minimum temperature of −1.49 °C at 15 m depth. This cold pool is characteristic of the ice mélange region, which extends 30 km into the

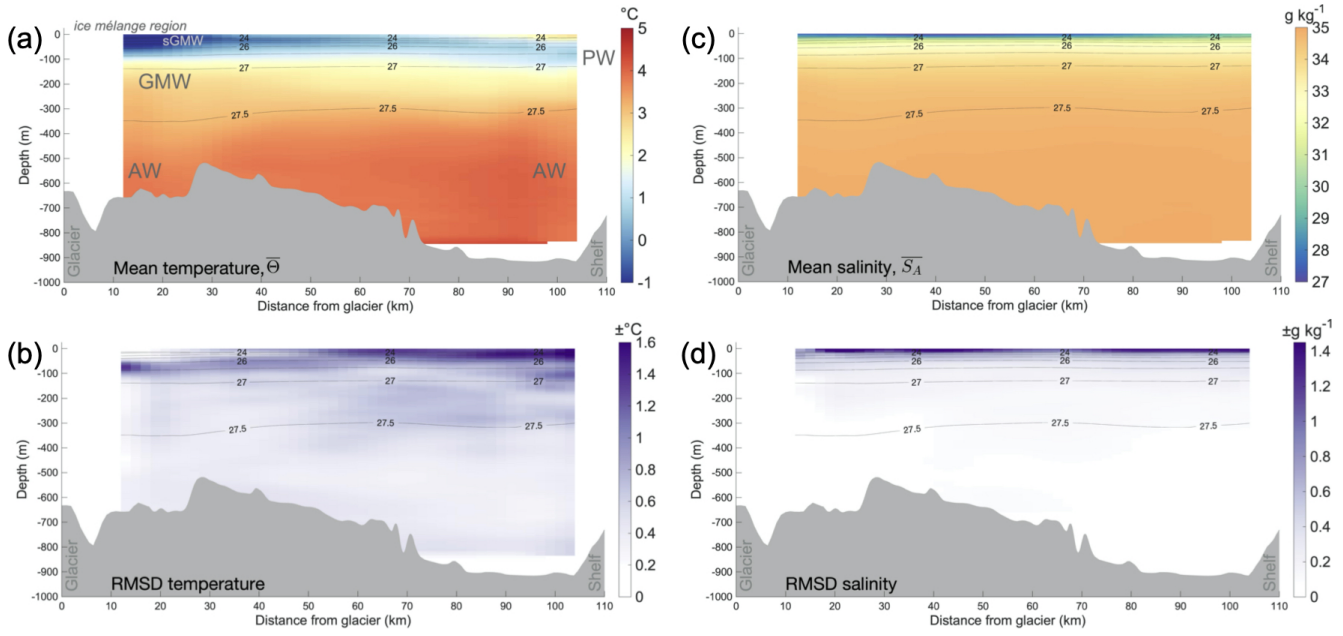

Figure 8. Gridded 13 year mean summer state climatology of conservative temperature **(a)** and absolute salinity **(b)** of the for Sermilik Fjord derived from hydrographic observations between 2009 to 2023. Associated RMSD about the mean for conservative temperature **(c)** and absolute salinity **(d)** show an estimate of spread of values in time at every grid cell. The $\sigma a_0 = 24$, 26, 27 and 27.5 kg m^{-3} potential density anomaly isopycnals are represented by grey contours in every panel and water masses discussed in the text (Atlantic Water (AW), glacially modified water (GMW), Polar Water (PW), and surface GMW (sGMW)) are labeled in panel **(a)**.

fjord. This also leads to the near glacier region showing the strongest thermocline (Fig. 10b–d) and, consequently, the strongest surface stratification of all the regions (Fig. 11b–d). Following Lindeman et al. (2024), we identify this as sGMW occurring at less than 50 m depth where $\sigma_0 < 26$ kg m^{-3}.

5.2.3 Mid-fjord properties

Considering the characteristics of the mid-fjord region (40–90 km from the glacier) in Θ–S_A space reveals that the water properties are a progressive mixture between the two end-members of the mouth and near glacier profiles (Fig. 9). We assume along-isopycnal mixing is occurring in the upper 400 m of the mid-fjord region ($\sigma_0 < 27.5$ g kg^{-1}) where GMW is being exported down the fjord and meeting waters of the same density coming into the fjord from the shelf. Above 50 m, the surface waters are warmer than the sGMW found in the mélange, with minimum temperatures above 0 °C.

The AW properties in the mid-fjord are similar to those at the mouth. The mid-fjord AW properties vertically averaged between 400–700 m and horizontally averaged between 60–70 km are 3.83 ± 0.05 °C and 34.90 ± 0.02 g kg^{-1}.

The middle of the fjord is at 60 km in the along-fjord distance coordinate axis. However, the map view of the fjord geometry is defined by a constriction at 75 km (at 65.60° N in Fig. 1) which influences the exchange of waters between the fjord mouth and upper fjord. Previous studies have described mooring records at this location (Jackson et al., 2014; Jackson and Straneo, 2016; Snow et al., 2023). To easily compare the findings of this study with the moored data, we define "mid-fjord" as 76 km. As Figs. 8 and 9 show, the water properties are similar between 60 and 76 km from the glacier.

5.3 Variability of gridded data

While the climatology shows the average summer hydrography, there is yearly variability and unique hydrographic patterns represented in the individual survey grids which are important to consider (see Supplement to view all yearly grids). The temporal RMSD of the properties climatology grids (Fig. 8c–d) provide an initial sense of the year-to-year variability in different regions of the fjord. Below 400 m, in the largely unmodified AW layer for the whole along-fjord domain, we see consistent RMSD values. The spatial average of the RMSD between 400–700 m and horizontally from 12–104 km are ±0.39 °C and ±0.06 g kg^{-1}.

The year-to-year variability above 400 m is relatively greater, with maximum RMSD values of both temperature and salinity occurring at the surface. While salinity RMSD vertical structure is similar between the fjord mouth to the near glacier region, the temperature RMSD vertical structure varies along the fjord above 400 m and most prominently in the surface layers.

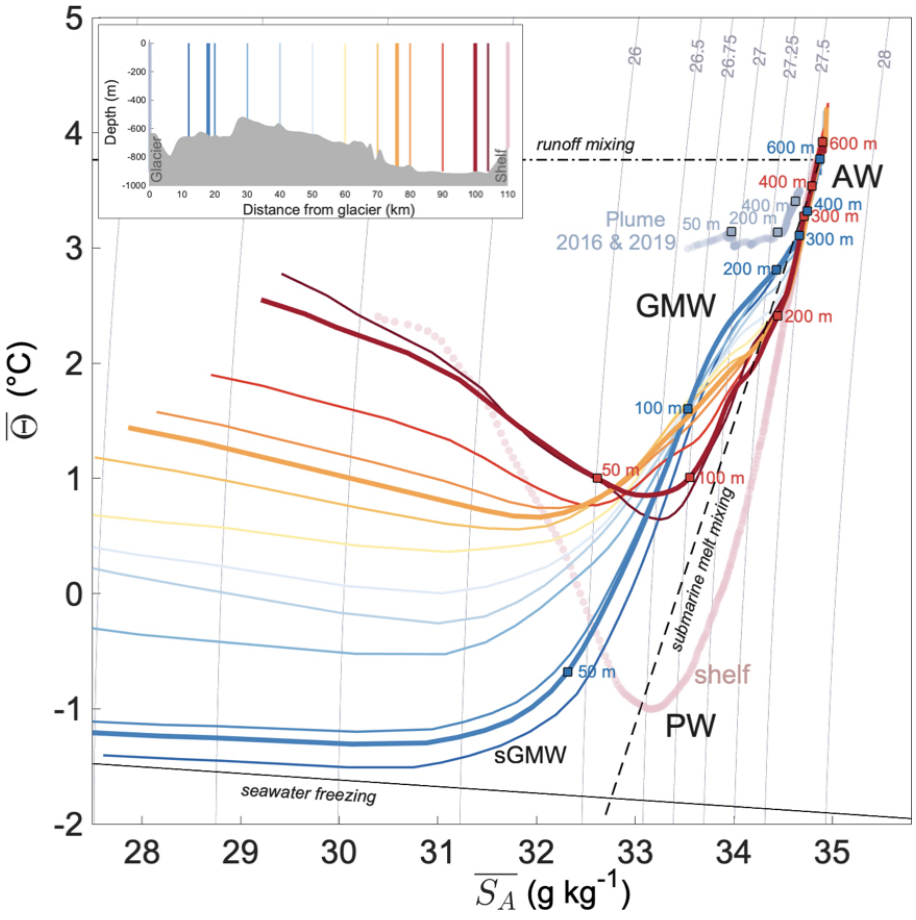

Figure 9. Conservative Temperature–Absolute Salinity (Θ–S_A) diagram of the gridded summer state climatology for Sermilik Fjord. Grid cells every 10 km in the along-fjord direction are plotted, with cool to warm colors representing increasing distance from the glacier terminus. Bold lines are representative of the three regions (mouth, mid-fjord, and near glacier) discussed in text and referred to in Figs. 10 and 11. The mean representative shelf profile is plotted in faded pink dots. The average of profiles from the subglacial discharge plume polyna in 2016 and 2019 are faded blue dots. Mixing lines are plotted for submarine ice melt (dashed line) and melt runoff (dot-dash line) and the seawater freezing line is the black solid line. Grey contours are potential density anomaly isopycnals. Water masses discussed in text (Atlantic Water (AW), glacially modified water (GMW), Polar Water (PW), and surface GMW (sGMW)) are labeled.

5.3.1 Fjord mouth variability

The mouth region shows the most variability from year to year in temperature properties (Fig. 8b). We speculate this is due to shelf processes, occurring on multiple timescales from seasonal to daily, influencing the properties measured at the mouth during a given field campaign (Jackson and Straneo, 2016; Jackson et al., 2018). While we showed that, on average, the fjord mouth temperature minimum is warmer than unmodified shelf PW, the 2015 and 2017 surveys have properties at the mouth that are equivalent to the unmodified shelf PW for those surveys. In other years (2010, 2018, 2019, 2020), more representative of the average, shelf PW properties are not present in the fjord and the fjord mouth temperatures are much warmer than shelf PW. Many of the mouth profiles show characteristic interleaving patterns above 200 m, where shelf and fjord GMW waters of similar density are meeting and mixing. Note that the average mouth profile is less smooth compared to the average near glacier profile due to multiple intrusions with sharp thermoclines at various depths being averaged together. This also impacts the stratification, which shows the largest range of yearly values between 50–200 m at the mouth (Fig. 11).

5.3.2 Near glacier variability

In the near glacier region, the upper 50 m has the smallest temperature RMSD of the fjord domain. This highlights the consistency of the ice mélange in setting the temperature properties in this area. From 50–100 m, there is an increase in the temperature RMSD (maximum $\pm$ 1.09 °C) as the thermocline is more variable – likely in response to variability in GMW extent in the water column and properties. Below the thermocline, the average RMSD of the GMW layer prop-

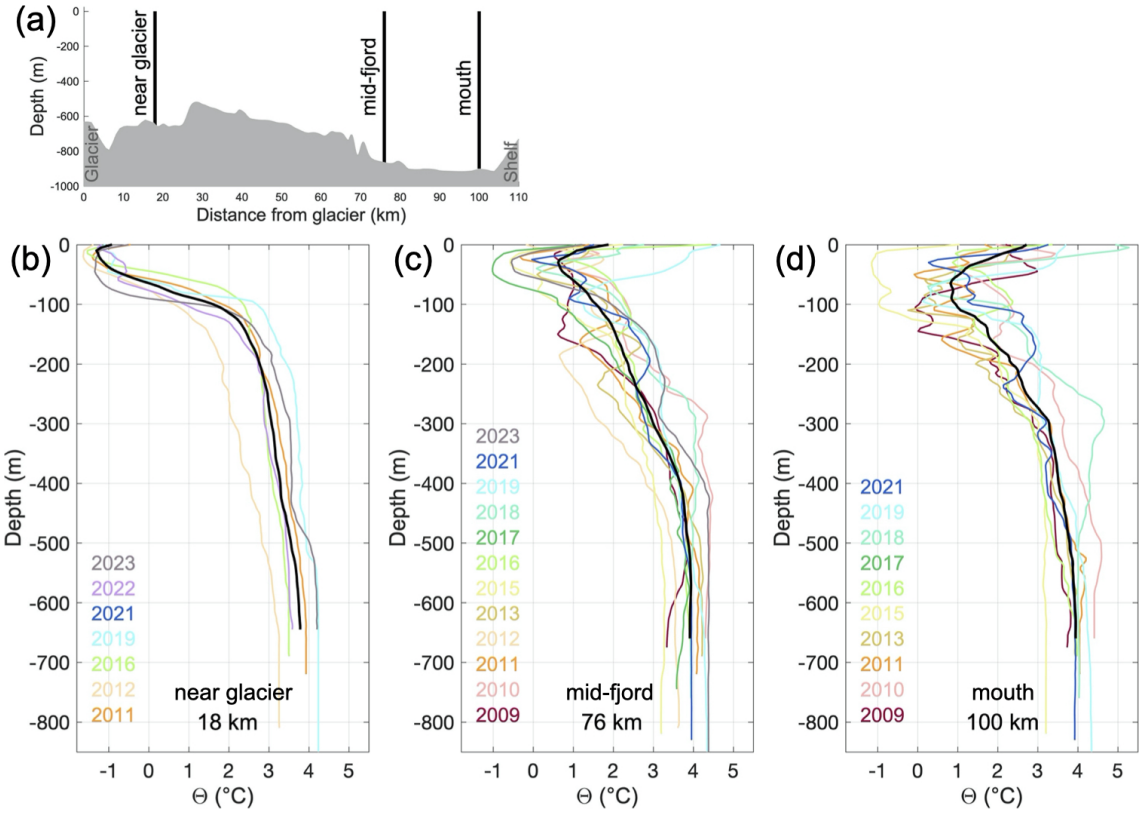

Figure 10. Conservative temperature profiles from all the yearly grids at locations shown in **(a)**: the near glacier **(b)**, mid-fjord **(c)**, and mouth regions **(d)**. Colored lines represent individual years and the bold black line is the time mean climatology profile.

erties between 165–300 m are $\pm 0.51\,^{\circ}\mathrm{C}$ and $\pm 0.14\,\mathrm{g\,kg^{-1}}$. As previous studies have noted, the properties of this GMW layer vary with the unmodified AW properties at depth near the glacier as these are the waters being upwelled (Muilwijk et al., 2022). When AW near the glacier is cooler (warmer) than average for a given year, the GMW properties resulting from upwelling in the SGD plume are cooler (warmer) than average.

5.3.3 Mid-fjord variability

Profiles from the mid-fjord region for each survey show similarly variable interleaving and intrusion features as the mouth profiles, though the mid-fjord intrusions are less sharp overall. Some years, properties in the mid-fjord region are more similar to an average near glacier profile (2015, 2017, 2023) with $< 0\,^{\circ}\mathrm{C}$ temperatures in the upper 50 m and exhibiting a strong thermocline between 50–100 m and relatively weak intrusions. Other years are more similar to a mouth profile (2011, 2012, 2021) with warmer surface waters and multiple stronger intrusions. The along-fjord location of the transition between near glacier properties and mouth properties varies from year to year. This variability is not captured in the time mean mid-fjord profile and climatology of the mid-fjord region.

5.3.4 Yearly anomalies from the mean

To further investigate the temporal variability, we subtracted the climatology from each summer grid to produce the temperature and salinity anomaly for each grid (selected years shown in Fig. 12). The temperature anomaly fields show summers where nearly the entire fjord domain is warmer (e.g. 2019) or colder (e.g. 2015) than average. 2021 is the year with the smallest average anomaly across the whole domain, however, there are still areas in the domain that are warmer and colder than the summer average.

The pattern in the gridded anomaly field can be both due to variability in the properties and variability in the depth of the thermocline. For example, the properties of the temperature minimum at the mouth could match the mean temperature minimum properties, but if the thermocline is at a different depth the anomaly will be nonzero.

6 Discussion

6.1 Summary of results facilitated by gridded sections

The method presented here, and the creation of gridded sections from discrete, irregular profiles, enables novel insights and quantification of water properties in Sermilik Fjord.

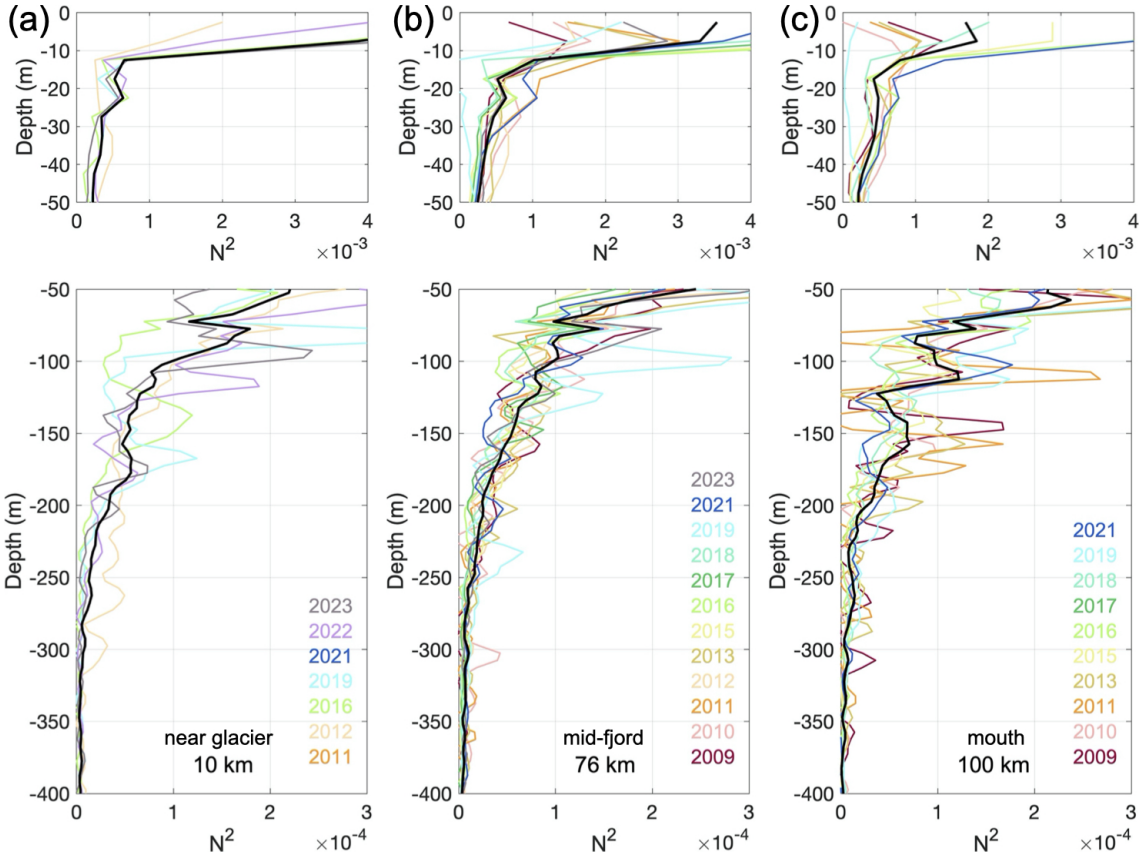

Figure 11. N^2 (Brunt–Vaisala frequency), a measure of stratification, from the near glacier **(a)**, mid-fjord **(b)**, and mouth **(c)** regions for all yearly gridded data. The profiles are from the same locations as in Fig. 10. The upper panels have a different vertical scale to emphasize the surface. The horizontal scale in the upper panels is an order of magnitude larger than the lower panels. N^2 was calculated from conservative temperature and absolute salinity gridded data using the TEOS-10 Oceanographic Toolbox (McDougall and Barker, 2011). Black bold lines represent the mean N^2 profile for all years in each region.

Most notably, the summer climatology product, along with complementary information on the range and patterns of variability, is only possible with regularly gridded sections and could not have been constructed from the original profiles alone. The same is true for the calculation of the anomalies relative to the climatological state, which allow direct interannual comparisons against a mean field. For example, our analysis shows that 2015 was an anomalously cold year in the fjord, suggesting that conclusions from previous studies based solely on 2015 data should be interpreted with caution.

Beyond climatology and anomalies, the gridded sections also reveal coherent fjord-scale property structures that are less evident in scattered profile data. For instance, variability in Atlantic Water along the fjord is more readily discerned in the gridded fields than in the raw profiles. The gridded format also enables straightforward calculation of spatially averaged water properties in different parts of the fjord, both for individual surveys and for the summer climatology. These mean properties, presented in the Results, are robust quantities that can be directly used in modeling and comparative studies. Together, these examples demonstrate that the gridded sections are not just improving the accessibility of the data, but also the interpretive power, producing results that would not otherwise be attainable.

Hydrographic data from fjords are relevant to a wide range of users – from climate and earth scientists interested in ice–ocean interactions to local communities that depend on the ecosystem. Our aim is to make this dataset both usable and useful across disciplines. In the following sections, we identify several important considerations regarding the use of these gridded data and the original profile observations.

6.2 Daily to interannual variability

While all the data are from the summer season (July–September), each along-fjord section is a snapshot capturing the combined influence of processes occurring on a range of timescales (days, months, years). Single wind events within the fjord and the adjacent shelf can influence fjord exchange and hydrographic properties over a timescale of days (Jackson and Straneo, 2016). Integrating data collected before and

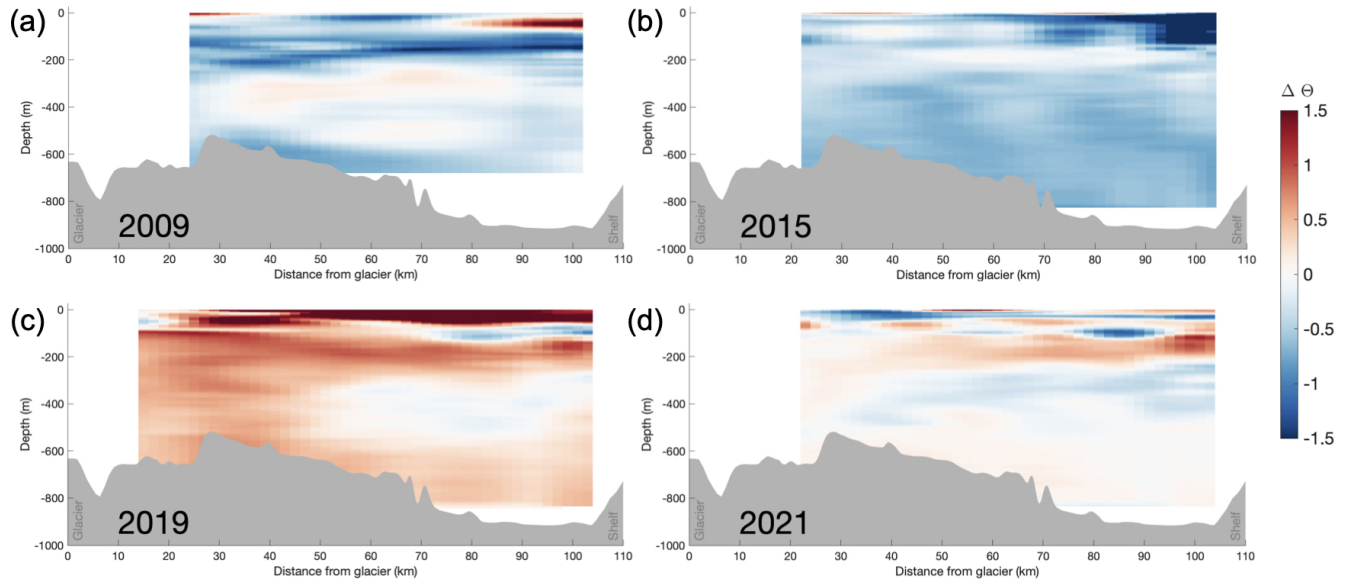

Figure 12. Conservative temperature anomalies from the climatological mean for yearly grids 2009 **(a)**, 2015 **(b)**, 2019 **(c)**, and 2021 **(d)**. Cooler (warmer) colors show values less (greater) than the mean for each grid cell.

after a single wind event during one survey can be challenging and creates discontinuities in the domain. Some profiles were not used in the construction of each along-fjord section because of these discontinuities.

All data and gridded products should also be interpreted within the context of the seasonal runoff cycle relative to the timing of data collection. Fjord properties change dramatically over the course of the surface melt season, with subglacial discharge input typically beginning in June and reaching its peak in August. Earlier studies have shown a progressive acceleration of fjord circulation, and associated modification of fjord properties, as a result of this seasonal forcing (Sanchez et al., 2023). For 2023, we did not combine the XCTD (collected on 12 July) and CTD (collected 9–16 August) surveys because the fjord properties had evolved significantly in the time between surveys. These data are treated as two different along-fjord sections. Because this data set incorporates sections collected at different points in the summer season (Fig. 3), the temporal variability reflects both interannual variability and the intraseasonal development of fjord conditions over the discharge period. Additionally, the high variability in properties directly at the surface (Fig. 8b, d) can be attributed to the variation of solar radiation forcing and terrestrial surface runoff (as opposed to subglacial discharge) at the seasonal timescale.

Variable regional atmospheric and ocean conditions occurring on larger spatial scales and longer time scales must also be considered. For example, in 2015, there was significant sea ice within the fjord and on the shelf during the summer survey, indicative of a prolonged winter. This is supported by findings that 2015 had an anonymously cold and long winter associated with a positive state of the North Atlantic Oscillation in Southeast Greenland and the Irminger Sea (de Jong and de Steur, 2016). Making any conclusions about interannual variability from this dataset must be done within the context of understanding the combined effect of these multiscale forcings on hydrographic patterns of each year. This will be the subject of future studies, and we are careful not to attribute hydrographic patterns discussed here to particular forcings as this requires further analysis outside the scope of this work.

6.3 Water mass definitions and comparison to previous work

The average summer water mass properties calculated here are consistent with previously reported definitions of summer AW, PW, and GMW in Sermilik Fjord from CTD, XCTD, and moored observations (Straneo et al., 2011; Jackson and Straneo, 2016; Beaird et al., 2018; Sanchez et al., 2021; Lindeman et al., 2024). Notably, CTD data from 2009 (Straneo et al., 2011), 2015 (Beaird et al., 2018), and 2021 (Lindeman et al., 2024) were used in previous studies to identify the properties and depth range of GMW in these individual years. Reinterpreting the conclusions of these previous results within the context of the climatological mean and long term dataset is now possible. For example, Beaird et al. (2018) relied on the 2015 CTD survey. We now know that this is a year when nearly the entire fjord domain was 1 °C colder than the 13 year climatological temperature mean (Fig. 12b).

How water mass properties are defined and averaged has varied between studies based on particular applications. Different isopycnal ranges, depths, and/or horizontal extents are

used to average and report water properties. The availability and format of the gridded sections allows a user to calculate any quantity they may need for a specific spatial extent or particular years based on the research question of interest. The gridded sections can also be combined with previously reported velocity data if a user wishes to calculate transport weighted means (Jackson and Straneo, 2016; Beaird et al., 2018).

6.4 Gridded products facilitate model use and comparison

Robust climatological means and consistently gridded surveys provide quantitative means for forcing or validating models. This is preferred over the use of single surveys or ad hoc choices made by earlier studies which used temperature and salinity profiles from Sermilik Fjord as initial conditions of idealized two-layer fjord models, boundary conditions and validation data for more complex numerical models, and ocean conditions for iceberg melt models and plume models (Sciascia et al., 2013; Moon et al., 2018; Davison et al., 2022; Schild et al., 2021; Sanchez et al., 2024). The gridded products presented here now make it easier to find average conditions for different fjord regions depending on the research question, model initialization, and time period of interest.

While we have not included the plume polynya profiles in the gridded products, the individual profiles are available in the original data and these can be useful in studies employing plume models. Similarly, the shelf profiles were not included in the gridded data presented here as the shelf environment dominated by different dynamics, but the individual profiles are available for use and provide important context for interpreting fjord water properties. We chose to create an average East section shelf profile to aid in the interpretation of properties at the fjord mouth. A more rigorous analysis of shelf water mass properties and the creation of a shelf summer climatology is possible with this dataset and will be considered in future work.

7 Code and data availability

The gridded data products for each individual year and the climatology are available at the Arctic Data Center (https://doi.org/10.18739/A2513TZ0P, https://doi.org/10.18739/A28G8FK6D, Roth et al., 2025a) and GitHub (https://github.com/a1roth/sermilik_gridded_hydrography, last access: 14 October 2025) as netCDF files. The files contain gridded section of Θ and S_A, as well as their respective mapping relative error matrices, for every summer survey. Derived variables, like potential density or N^2, can be calculated by the user. The thalweg along-fjord gridded coordinates in distance (km) from the 2019 Helheim Glacier terminus position and in latitude and longitude coordinates are included in the files.

The original CTD and XCTD profiles from every year of sampling are all available at the Arctic Data Center as netCDF files (https://arcticdata.io/catalog/portals/sermilik/Data, last access: 14 October 2025, Straneo et al., 2025). Individual entries and DOIs have been created for each field campaign. All files include in situ temperature and practical salinity. Some years have additional variables from the CTD rosette, such as dissolved oxygen and turbidity. All files include latitude and longitude coordinates of every profile and standardized depth levels (meters). As more hydrographic surveys are conducted in Sermilik Fjord, we plan for the data to be archived in this format and available at the Arctic Data Center in the Sermilik Hydrography Data Portal (https://arcticdata.io/catalog/portals/sermilik, last access: 14 October 2025, Straneo et al., 2025).

The code developed to create gridded along-fjord sections is available at GitHub (https://doi.org/10.5281/zenodo.17563180, Roth et al., 2025b). While this code is set up for Sermilik Fjord profiles, it can easily be adapted to other regions with discrete profiles that have been compiled into along-fjord sections. The parameters of the objective mapping method can be manually adjusted for different length scales and error input. Ancillary code for plotting and deriving other variables is also available (Roth et al., 2025b).

8 Conclusions

The dataset and gridded products presented in this study provide a crucial step toward standardizing and centralizing long-term fjord observations in Greenland. By compiling 13 years of hydrographic data from Sermilik Fjord, we offer a comprehensive and accessible resource for studying fjord dynamics and ice–ocean interactions. The combined CTD and XCTD observations lead to greater spatial coverage of the fjord, including the mélange region for multiple years and the subglacial discharge plume polyna region for two years. The objective mapping method enabled necessary and novel analyses that are not possible from the raw profiles alone, including the construction of an along-fjord summer climatology, quantification of interannual anomalies, and identification of water property features. Importantly, these results provide context for interpreting previous work in Sermilik Fjord. We demonstrated how other quantities (e.g. N^2) and water properties of specific regions can easily be calculated from the gridded sections depending on questions of interest. Finally, the method used to generate gridded sections is adaptable for different variables and fjord settings and can facilitate interdisciplinary research – enabling comparisons with models, biological data, and other observations.

This work highlights the need for a coordinated approach to fjord data collection and sharing. Establishing a structured, FAIR-compliant data repository for Greenland fjords will improve the accessibility and utility of these critical datasets,

ultimately enhancing our understanding of glacial fjord systems and strengthening collaboration within the international science community and with Greenlandic partners.

Supplement. The supplement related to this article is available online at https://doi.org/10.5194/essd-17-6025-2025-supplement.

Author contributions. All authors designed and conceptualized the study. AR led the study, data processing, and writing of the manuscript. FS initiated and has led the data collection, processing, and research activities in Sermilik Fjord since 2008. FS, JH, and ML have all substantially contributed to data processing, archiving, and manuscript writing. MM contributed code and guidance for the objective mapping method and contributed to manuscript writing.

Competing interests. The contact author has declared that none of the authors has any competing interests.

Disclaimer. Publisher's note: Copernicus Publications remains neutral with regard to jurisdictional claims made in the text, published maps, institutional affiliations, or any other geographical representation in this paper. While Copernicus Publications makes every effort to include appropriate place names, the final responsibility lies with the authors. Views expressed in the text are those of the authors and do not necessarily reflect the views of the publisher.

Acknowledgements. The authors thank the many crew members, scientists, technicians, and logistics staff who have supported data collection efforts since 2008. These data would not exist if it were not for the knowledge and skill of the ships' crewmembers, most of them Greenlandic, including those of the M/Vs *Viking*, Adolf Jensen and R/V *Tarajoq*. The XCTD data were collected thanks to the patience and expertise of the many helicopter pilots, mostly from Air Greenland. FS acknowledges the essential role played by the late Gordon Hamilton in motivating and initiating the collection of these data. We acknowledge the many scientists who contributed to this data collection. In particular, we acknowledge the contributions of D. Sutherland, R. Jackson, N. Beaird, M. Andres, D. Slater, L. Stearns, A. Lewinter, D. Finnegan and the late G. Hamilton. Invaluable technical support was provided by A. Ramsey, J. Ryder, W. Ostrom, M. Donahue and J. Kemp's entire group. Finally, we thank two anonymous reviewers for their time and contributions to improving the manuscript.

Successfully accomplishing and funding this work has required coordination and collaboration with multiple research groups across disciplines as we seek to answer increasingly complex and socially relevant questions. Maintaining positive collaboration with other research groups, Greenland-based scientists, logistics personnel, research vessels, and local people has been essential to ensuring observations are funded and conducted year after year.

Financial support. This research has been supported by the Heising-Simons Foundation, the US National Science Foundation (Grant numbers: 0909373, 1130008, 1332911, 1434041, 1657601, and 2127241), and the Kerr Foundation.

Review statement. This paper was edited by Davide Bonaldo and reviewed by two anonymous referees.

References

Beaird, N. L., Straneo, F., and Jenkins, W.: Export of Strongly Diluted Greenland Meltwater From a Major Glacial Fjord, Geophysical Research Letters, 45, 4163–4170, https://doi.org/10.1029/2018GL077000, 2018.

Bjørk, A. A., Kruse, L. M., and Michaelsen, P. B.: Brief communication: Getting Greenland's glaciers right – a new data set of all official Greenlandic glacier names, The Cryosphere, 9, 2215–2218, https://doi.org/10.5194/tc-9-2215-2015, 2015.

Bretherton, F. P., Davis, R. E., and Fandry, C.: A technique for objective analysis and design of oceanographic experiments applied to MODE-73, Deep Sea Research and Oceanographic Abstracts, 23, 559–582, https://doi.org/10.1016/0011-7471(76)90001-2, 1976.

Cape, M. R., Straneo, F., Beaird, N., Bundy, R. M., and Charette, M. A.: Nutrient release to oceans from buoyancy-driven upwelling at Greenland tidewater glaciers, Nature Geoscience, 12, 34–39, https://doi.org/10.1038/s41561-018-0268-4, 2019.

Davison, B. J., Cowton, T., Sole, A., Cottier, F., and Nienow, P.: Modelling the effect of submarine iceberg melting on glacier-adjacent water properties, The Cryosphere, 16, 1181–1196, https://doi.org/10.5194/tc-16-1181-2022, 2022.

de Jong, M. F. and de Steur, L.: Strong winter cooling over the Irminger Sea in winter 2014–2015, exceptional deep convection, and the emergence of anomalously low SST, Geophysical Research Letters, 43, 7106–7113, https://doi.org/10.1002/2016GL069596, 2016.

Dotto, T. S., Mata, M. M., Kerr, R., and Garcia, C. A. E.: A novel hydrographic gridded data set for the northern Antarctic Peninsula, Earth Syst. Sci. Data, 13, 671–696, https://doi.org/10.5194/essd-13-671-2021, 2021.

Enderlyn, E. M., Hamilton, G. S., Straneo, F., and Sutherland, D. A.: Iceberg meltwater fluxes dominate the freshwater budget in Greenland's iceberg-congested glacial fjords, Geophysical Research Letters, 43, 11287–11294, https://doi.org/10.1002/2016GL070718, 2016.

Foga, S.: Characterization of Ice Mélange and its Implications toTerminus Stability at Helheim Glacier, Southeast Greenland, Master's thesis, University of Kansas, Lawerence, KS, https://core.ac.uk/reader/213418374 (last access: 12 December 2024), 2016.

Gade, H. G.: Melting of Ice in Sea Water: A Primitive Model with Application to the Antarctic Ice Shelf and Icebergs, Journal of Physical Oceanography, 9, 189–198, https://doi.org/10.1175/1520-0485(1979)009<0189:MOIISW>2.0.CO;2, 1979.

Harcourt, W. D., Shahin, M. G., Stearns, L. A., and Shankar, S.: Structural weaknesses in ice mélange revealed by high-

resolution ICEYE SAR imagery, Journal of Glaciology, 1–32, https://doi.org/10.1017/jog.2025.10085, 2025.

Harden, B. E., Straneo, F., and Sutherland, D. A.: Moored observations of synoptic and seasonal variability in the East Greenland Coastal Current, Journal of Geophysical Research: Oceans, 119, 8838–8857, https://doi.org/10.1002/2014JC010134, 2014.

Holm, L.: Sila-Inuk: Study of the Impacts of Climate Change in Greenland, 145–160, ISBN 978-90-481-8586-3, https://doi.org/10.1007/978-90-481-8587-0_6, 2010.

Hopwood, M. J., Carroll, D., Dunse, T., Hodson, A., Holding, J. M., Iriarte, J. L., Ribeiro, S., Achterberg, E. P., Cantoni, C., Carlson, D. F., Chierici, M., Clarke, J. S., Cozzi, S., Fransson, A., Juul-Pedersen, T., Winding, M. H. S., and Meire, L.: Review article: How does glacier discharge affect marine biogeochemistry and primary production in the Arctic?, The Cryosphere, 14, 1347–1383, https://doi.org/10.5194/tc-14-1347-2020, 2020.

Howat, I. M., Negrete, A., and Smith, B. E.: The Greenland Ice Mapping Project (GIMP) land classification and surface elevation data sets, The Cryosphere, 8, 1509–1518, https://doi.org/10.5194/tc-8-1509-2014, 2014.

Hughes, K. G.: Pathways, Form Drag, and Turbulence in Simulations of an Ocean Flowing Through an Ice Mélange, Journal of Geophysical Research: Oceans, 127, e2021JC018228, https://doi.org/10.1029/2021JC018228, 2022.

Huiban, F., Millan, R., Kjeldsen, K. K., Andresen, C. S., Dømgaard, M., Dehecq, A., Brunt, S., Khan, S. A., Mouginot, J., and Bjørk, A. A.: Regional ice flow piracy following the collapse of Midgaard Glacier in Southeast Greenland, Nature Communications, 15, 9976, https://doi.org/10.1038/s41467-024-54045-z, 2024.

Ide, K., Courtier, P., Ghil, M., and Lorenc, A. C.: Unified Notation for Data Assimilation: Operational, Sequential and Variational (gtSpecial IssueltData Assimilation in Meteology and Oceanography: Theory and Practice), Journal of the Meteorological Society of Japan Ser. II, 75, 181–189, https://doi.org/10.2151/jmsj1965.75.1B_181, 1997.

Jackson, R. H. and Straneo, F.: Heat, Salt, and Freshwater Budgets for a Glacial Fjord in Greenland, Journal of Physical Oceanography, 46, 2735–2768, https://doi.org/10.1175/JPO-D-15-0134.1, 2016.

Jackson, R. H., Straneo, F., and Sutherland, D. A.: Externally forced fluctuations in ocean temperature at Greenland glaciers in non-summer months, Nature Geoscience, 7, 503–508, https://doi.org/10.1038/ngeo2186, 2014.

Jackson, R. H., Lentz, S. J., and Straneo, F.: The Dynamics of Shelf Forcing in Greenlandic Fjords, Journal of Physical Oceanography, 48, 2799–2827, https://doi.org/10.1175/JPO-D-18-0057.1, 2018.

Juul-Pedersen, T., Rysgaard, S., Batty, P., Mortensen, J., Retzel, A., Nygaard, R., Burmeister, A., Mikkelsen, D. M., Sejr, M. K., Blicher, M. E., Krause-Jensen, D., Christensen, P. B., Labansen, A. L., Rasmussen, L. M., Simon, M., Boye, T. K., Madsen, P. T., and Ugarte, F.: NUUK BASIC: The MarineBasis Programme, in: Nuuk Ecological Research Operations, edited by: Jensen, L. M. and Rasch, M., National Environmental Research Institute, Aarhus University, Aarhus, Denmark, 39–58, ISBN 978-87-7073-125-6, 2009.

Laidre, K. L., Supple, M. A., Born, E. W., Regehr, E. V., Øystein Wiig, Ugarte, F., Aars, J., Dietz, R., Sonne, C., Hegelund, P., Isaksen, C., Akse, G. B., Cohen, B., Stern, H. L., Moon, T., Vollmers, C., Corbett-Detig, R., Paetkau, D., and Shapiro, B.: Glacial ice supports a distinct and undocumented polar bear subpopulation persisting in late 21st-century sea-ice conditions, Science, 376, 1333–1338, https://doi.org/10.1126/science.abk2793, 2022.

Lindeman, M., Straneo, F., Adams, H., Nelson, M., and Schartup, A.: Low mercury concentrations in a Greenland glacial fjord attributed to oceanic sources, Nature Communications Earth and Environment, 5, https://doi.org/10.1038/s43247-024-01474-9, 2024.

Mankoff, K. D., Noël, B., Fettweis, X., Ahlstrøm, A. P., Colgan, W., Kondo, K., Langley, K., Sugiyama, S., van As, D., and Fausto, R. S.: Greenland liquid water discharge from 1958 through 2019, Earth Syst. Sci. Data, 12, 2811–2841, https://doi.org/10.5194/essd-12-2811-2020, 2020.

Mazloff, M. R., Verdy, A., Gille, S. T., Johnson, K. S., Cornuelle, B. D., and Sarmiento, J.: Southern Ocean Acidification Revealed by Biogeochemical-Argo Floats, Journal of Geophysical Research: Oceans, 128, e2022JC019530, https://doi.org/10.1029/2022JC019530, 2023.

McDougall, T. and Barker, P.: Getting started with TEOS-10 and the Gibbs Seawater (GSW) Oceanographic Toolbox, https://www.teos-10.org/software.htm (last access: 3 March 2021), 2011.

Meire, L., Mortensen, J., Meire, P., Juul-Pedersen, T., Sejr, M. K., Rysgaard, S., Nygaard, R., Huybrechts, P., and Meysman, F. J. R.: Marine-terminating glaciers sustain high productivity in Greenland fjords, Global Change Biology, 23, 5344–5357, https://doi.org/10.1111/gcb.13801, 2017.

Melton, S. M., Alley, R. B., Anandakrishnan, S., Parizek, B. R., Shahin, M. G., Stearns, L. A., Lewinter, A. L., and Finnegan, D. C.: Meltwater drainage and iceberg calving observed in high-spatiotemporal resolution at Helheim Glacier, Greenland, Journal of Glaciology, 68, 812–828, https://doi.org/10.1017/jog.2021.141, 2022.

Meng, Y., Lai, C.-Y., Culberg, R., Shahin, M. G., Stearns, L. A., Burton, J. C., and Nissanka, K.: Seasonal changes of mélange thickness coincide with Greenland calving dynamics, Nature Communications, 16, 573, https://doi.org/10.1038/s41467-024-55241-7, 2025.

Moon, T., Sutherland, D., Carroll, D., Felikson, D., Kehrl, L., and Straneo, F.: Subsurface iceberg melt key to Greenland fjord freshwater budget, Nature Geoscience, 11, 49–54, https://doi.org/10.1038/s41561-017-0018-z, 2018.

Morlighem, M., Williams, C. N., Rignot, E., An, L., Arndt, J. E., Bamber, J. L., Catania, G., Chauché, N., Dowdeswell, J. A., Dorschel, B., Fenty, I., Hogan, K., Howat, I., Hubbard, A., Jakobsson, M., Jordan, T. M., Kjeldsen, K. K., Millan, R., Mayer, L., Mouginot, J., Noël, B. P. Y., O'Cofaigh, C., Palmer, S., Rysgaard, S., Seroussi, H., Siegert, M. J., Slabon, P., Straneo, F., van den Broeke, M. R., Weinrebe, W., Wood, M., and Zinglersen, K. B.: BedMachine v3: Complete bed topography and ocean bathymetry mapping of Greenland from multibeam echo sounding combined with mass conservation, Geophys. Res. Lett., 44, 11051–11061, https://doi.org/10.1002/2017GL074954, 2017.

Mortensen, J., Rysgaard, S., Arendt, K., Juul-Pedersen, T., Søgaard, D., Bendtsen, J., and Meire, L.: Local Coastal Water Masses Control Heat Levels in a West Greenland Tidewater Out-

let Glacier Fjord, Journal of Geophysical Research: Oceans, 123, 8068–8083, https://doi.org/10.1029/2018JC014549, 2018.

Muilwijk, M., Straneo, F., Slater, D. A., Smedsrud, L. H., Holte, J., Wood, M., Andresen, C. S., and Harden, B.: Export of Ice Sheet Meltwater from Upernavik Fjord, West Greenland, Journal of Physical Oceanography, 52, 363–382, https://doi.org/10.1175/JPO-D-21-0084.1, 2022.

Nuttall, M.: Water, ice, and climate change in northwest Greenland, WIREs Water, 7, e1433, https://doi.org/10.1002/wat2.1433, 2020.

Rathcke, K., Qatsa, M., Burdenski, A., and Jacobsen, R.: Understanding marine biodiversity shifts in Southeast Greenland with Indigenous and local knowledge, Human Ecology: An Interdisciplinary Journal, 53, 29–40, https://doi.org/10.1007/s10745-025-00570-4, 2025.

Reeve, K. A., Boebel, O., Kanzow, T., Strass, V., Rohardt, G., and Fahrbach, E.: A gridded data set of upper-ocean hydrographic properties in the Weddell Gyre obtained by objective mapping of Argo float measurements, Earth Syst. Sci. Data, 8, 15–40, https://doi.org/10.5194/essd-8-15-2016, 2016.

Roemmich, D.: Optimal Estimation of Hydrographic Station Data and Derived Fields, Journal of Physical Oceanography, 13, 1544–1549, https://doi.org/10.1175/1520-0485, 1983.

Roth, A., Straneo, F., Holte, J., Lindeman, M., and Mazloff, M.: Gridded hydrographic dataset for Sermilik Fjord, Southeast Greenland from 2009–2023, Arctic Data Center [data set], https://doi.org/10.18739/A28G8FK6D, 2025a.

Roth, A., Straneo, F., Holte, J., Lindeman, M., and Mazloff, M.: Sermilik Gridded Hydrography v1, Zenodo [code], https://doi.org/10.5281/zenodo.17563180, 2025b.

Sanchez, R., Slater, D., and Straneo, F.: Delayed Freshwater Export from a Greenland Tidewater Glacial Fjord, Journal of Physical Oceanography, 53, 1291–1309, https://doi.org/10.1175/JPO-D-22-0137.1, 2023.

Sanchez, R., Straneo, F., and Andres, M.: Using Acoustic Travel Time to Monitor the Heat Variability of Glacial Fjords, J. Atmos. Oceanic Technol., 38, 1535–1550, https://doi.org/10.1175/JTECH-D-20-0176.1, 2021.

Sanchez, R., Straneo, F., Hughes, K., Barbour, P., and Shroyer, E.: Relative Roles of Plume and Coastal Forcing on Exchange Flow Variability of a Glacial Fjord, Journal of Geophysical Research: Oceans, 129, e2023JC020492, https://doi.org/10.1029/2023JC020492, 2024.

Schild, K. M., Sutherland, D. A., Elosegui, P., and Duncan, D.: Measurements of Iceberg Melt Rates Using High-Resolution GPS and Iceberg Surface Scans, Geophysical Research Letters, 48, e2020GL089765, https://doi.org/10.1029/2020GL089765, 2021.

Schiøtt, S., Tejsner, P., and Rysgaard, S.: Inuit and Local Knowledge on The Marine Ecosystem in Ilulissat Icefjord, Greenland, Human Ecology, 50, 167–181, https://doi.org/10.1007/s10745-021-00277-2, 2022.

Schlegel, R. W. and Gattuso, J.-P.: A dataset for investigating socio-ecological changes in Arctic fjords, Earth Syst. Sci. Data, 15, 3733–3746, https://doi.org/10.5194/essd-15-3733-2023, 2023.

Sciascia, R., Straneo, F., Cenedese, C., Heimbach, P., Ribergaard, M. H., Mortensen, J., and Muench, R. D.: Seasonal variability of submarine melt rate and circulation in an East Greenland fjord, Journal of Geophysical Research: Oceans, 118, 2492–2506, https://doi.org/10.1002/jgrc.20142, 2013.

Snow, T., Zhang, W., Schreiber, E., Siegfried, M., Abdalati, W., and Scambos, T.: Alongshore winds force warm Atlantic Water toward Helheim Glacier in southeast Greenland, Journal of Geophysical Research: Oceans e2023JC019953, https://doi.org/10.1029/2023JC019953, 2023.

Spall, M. A., Jackson, R. H., and Straneo, F.: Katabatic Wind-Driven Exchange in Fjords, Journal of Geophysical Research: Oceans, 122, 8246–8262, https://doi.org/10.1002/2017JC013026, 2017.

Straneo, F. and Cenedese, C.: The Dynamics of Greenland's Glacial Fjords and Their Role in Climate, Annual Review of Marine Science, 7, 89–112, https://doi.org/10.1146/annurev-marine-010213-135133, 2015.

Straneo, F., Hamilton, G. S., Sutherland, D. A., Stearns, L. A., Davidson, F., Hammill, M. O., Stenson, G. B., and Rosing-Asvid, A.: Rapid circulation of warm subtropical waters in a major glacial fjord in East Greenland, Nature Geoscience, 3, 182–186, https://doi.org/10.1038/ngeo764, 2010.

Straneo, F., Curry, R., Sutherland, D., Hamilton, G., Cenedese, C., Vaage, K., and Stearns, L.: Impact of ocean stratification on submarine melting of a major Greenland outlet glacier, Nature Precedings, https://doi.org/10.1038/npre.2011.5670.1, 2011.

Straneo, F., Sutherland, D., Holland, D., Gladish, C., Hamilton, G. S., Johnson, H. L., Rignot, E., Xu, Y., and Koppes, M.: Characteristics of ocean waters reaching Greenland's glaciers, Annals of Glaciology, 53, 202–210, https://doi.org/10.3189/2012AoG60A059, 2012.

Straneo, F., Hamilton, G. S., Stearns, L. A., and Sutherland, D. A.: Connecting the Greenland Ice Sheet and the Ocean: A CASE STUDY OF HELHEIM GLACIER AND SERMILIK FJORD, Oceanography, 29, 34–45, https://www.jstor.org/stable/24862280 (last access: 21 April 2023), 2016.

Straneo, F., Sutherland, D., Stearns, L., and Catania, G.: Frontiers | The Case for a Sustained Greenland Ice Sheet-Ocean Observing System (GrIOOS), Front. Mar. Sci., 29, https://doi.org/10.3389/fmars.2019.00138, 2019.

Straneo, F., Slater, D., Bouchard, C., Cape, M., Carey, M., Ciannelli, L., Holte, J., Matrai, P., Laidre, K., Little, C., Meire, L., Seroussi, H., and Vernet, M.: An Interdisciplinary Perspective on Greenland's Changing Coastal Margins, Oceanography, https://doi.org/10.5670/oceanog.2022.128, 2022.

Straneo, F., Roth., A., Holte, J., and Lindeman, M.: Sermilik Fjord Hydrography Data Portal, Arctic Data Center, https://arcticdata.io/catalog/portals/sermilik/Overview (last access: 7 November 2025), 2025.

Sugiyama, S., Yamaguchi, A., Watanabe, T., Tojo, Y., Hayashi, N., Thiebot, J.-B., Tomiyasu, M., Hasegawa, K., Mitani, Y., Ogawa, M., Tanaka, K., Sakurai, K., Matsuno, K., Kanna, N., Podolskiy, E., Kusaka, R., Wang, Y., Imazu, Y., Watanabe, K., Sato, K., Ukai, S., Yamada, S., Kondo, K., Yamasaki, S., Tateyama, K., Sato, K., Inoue, J., Mori, T., Fukazawa, T., Rosing-Asvid, A., Langley, K., Gierisch, A. M. U., Sutherland, J., and Oshima, T.: Rapidly changing glaciers, ocean and coastal environments, and their impact on human society in the Qaanaaq region, northwestern Greenland, Polar Science, 27, 100632, https://doi.org/10.1016/j.polar.2020.100632, 2020.

Sugiyama, S., Yamaguchi, A., Watanabe, T., Tojo, Y., Hayashi, N., Thiebot, J., Tomiyasu, M., Hasegawa, K., Mitani, Y., Ogawa, M., Tanaka, K., Sakurai, K., Matsuno, K., Kanna, N., Podolskiy, E., Kusaka, R., Wang, Y., Imazu, Y., Watanabe, K., Sato, K., Ukai, S., Yamada, S., Kondo, K., Yamasaki, S., Tateyama, K., Sato, K., Inoue, J., Mori, T., Fukazawa, T., Rosing-Asvid, A., Langley, K., Gierisch, A. M. U., Sutherland, J., and Oshima, T.: Changes in the coastal environments and their impact on society in the Qaanaaq region, northwestern Greenland, Polar Science, 101206, https://doi.org/10.1016/j.polar.2025.101206, 2025.

Sutherland, D. A. and Pickart, R. S.: The East Greenland Coastal Current: Structure, variability, and forcing, Progress in Oceanography, 78, 58–77, https://doi.org/10.1016/j.pocean.2007.09.006, 2008.

Sutherland, D. A., Roth, G. E., Hamilton, G. S., Mernild, S. H., Stearns, L. A., and Straneo, F.: Quantifying flow regimes in a Greenland glacial fjord using iceberg drifters, Geophysical Research Letters, 41, 8411–8420, https://doi.org/10.1002/2014GL062256, 2014a.

Sutherland, D. A., Straneo, F., and Pickart, R. S.: Characteristics and dynamics of two major Greenland glacial fjords, Journal of Geophysical Research: Oceans, 119, 3767–3791, https://doi.org/10.1002/2013JC009786, 2014b.

Williams, J. J., Gourmelen, N., Nienow, P., Bunce, C., and Slater, D.: Helheim Glacier Poised for Dramatic Retreat, Geophysical Research Letters, 48, e2021GL094546, https://doi.org/10.1029/2021GL094546, 2021.

Wong, A. P. S., Johnson, G. C., and Owens, W. B.: Delayed-Mode Calibration of Autonomous CTD Profiling Float Salinity Data by θ–S Climatology, Journal of Atmospheric and Oceanic Technology, 20, 308–318, https://doi.org/10.1175/1520-0426(2003)020<0308:DMCOAC>2.0.CO;2, 2003.